Sedimentary Geology 453 (2023) 106440

Contents lists available at ScienceDirect

Sedimentary Geology

journal homepage: www.elsevier.com/locate/sedgeo

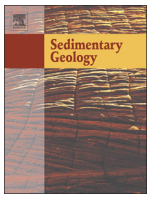

Geochemical approach for decoding the paleoenvironmental and depositional evolution of a coastal lacustrine Konservat-Lagerstätte (Early Cretaceous, south-Central Pyrenees)

Alejandro Gil-Delgado [a,f], David Cruset [b], Oriol Oms [a], Edgar Botero [c], Jordi Ibáñez-Insa [b], Xavier Delclòs [d], Albert Sellés [e,f], Àngel Galobart [e,f], Ramon Mercedes-Martín [a,*]

[a] Universitat Autònoma de Barcelona, Geology Department, Edifici Cs, 08193 Cerdanyola del Vallès, Spain
[b] Geosciences Barcelona (GEO3BCN-CSIC), Lluís Solé i Sabarís, s/n, 08028 Barcelona, Spain
[c] Technische Universitaat Hamburg-Harburg, Institute of River and Coastal Engineering, Am Schwarzenber g-Campus 1, 21073 Hamburg, Germany
[d] Universitat de Barcelona, Faculty of Earth Sciences, Department of Earth and Ocean Dynamics, C/i Franquès s/n, 08028 Barcelona, Spain
[e] Institut Català de Paleontologia Miquel Crusafont, C/ Escola Industrial, 23, 08201 Sabadell, Spain
[f] Museu de la Conca Dellà, C/ del museu, 4, 25650 Isona i Conca Dellà, Spain

ARTICLE INFO

Article history:
Received 16 March 2023
Received in revised form 22 May 2023
Accepted 23 May 2023
Available online 29 May 2023

Editor: Dr. Brian Jones

Keywords:
Fossil lagerstätte
Lacustrine carbonates
Stable isotopes
Multiproxy geochemistry

ABSTRACT

The lithographic limestone of La Pedrera de Meià (LPM) in south-Central Pyrenees (NE Spain) is considered one of the best preserved lacustrine-coastal successions of the Early Cretaceous in Europe, hosting a taxonomically diverse record of Barremian biota. While this Konservat-Lagerstätte has been extensively surveyed for paleontological purposes, little is known about the paleoenvironmental and depositional conditions prevailing during the formation of this fossil lagerstätte deposit. LPM limestone is made up of a homogeneous, dark gray to pale brown, faintly laminated 50 m-thick succession of micrite-rich intervals. To shed light on the environmental conditions of deposition, 303 rock samples were studied using a multiproxy approach based on different techniques including petrography, SEM-EDX, XRD, ICP-MS, XRF, Rare Earth Element distributions and C and O stable isotope geochemistry. The combination of sedimentological and geochemical data reveals a vertical shift of facies from littoral to profundal environments and then returning to littoral conditions. Profundal facies are made up of filament-rich mudstones originated from in situ precipitation of micrite either through biotically mediated or physico-chemical processes in undisturbed low energy settings, under anoxic conditions, characterized by the presence of transported terrestrial and lacustrine organisms that are exquisitely well-preserved. Littoral areas are characterized by the presence of in situ charophytes, smooth ostracods, and miliolid foraminifera that accumulated in mud-rich facies indicating low/moderate-energy, shallow-water, and relatively oxygenated conditions. Stable isotopic data and elemental geochemistry suggest a hydrologically closed to semi-closed lacustrine system with a restricted water circulation encouraging dysoxic to anoxic conditions in profundal sediments. Paleoproductivity proxies suggest a good correlation between catchment-derived siliciclastic discharge to the lake and primary productivity peaks. Furthermore, a decline in terrigenous input coupled with a reduction of meteoric water entrance to the lake is interpreted based on elemental proxies derived from paleosalinity and paleoredox analysis. Collectively, the strontium/barium (Sr/Ba) ratios, the sparse presence of miliolid foraminifera, and the isotopic signatures indicate an increase in salinity toward the younger intervals of the lake infilling, although their ultimate causes are unclear (i.e., increased evaporation, or a combination of reduced meteoric input and sporadic marine inputs might explain our data). The present work shows the importance of performing detailed multiproxy geochemical-sedimentological studies to better constrain the unique paleoenvironmental and paleohydrological conditions associated with the exceptional preservation of fossil biotas in Konservat-Lagerstätte deposits in analogous depositional settings.

1. Introduction

Konservat-Lagerstätte deposits are fossil accumulations characterized by the exceptional preservation of their biomineralized remains

* Corresponding author.
E-mail address: ramon.mercedes@uab.cat (R. Mercedes-Martín).

https://doi.org/10.1016/j.sedgeo.2023.106440

(e.g., shells, carcasses) and/or soft-tissues (e.g., organs, cellular structures) (Clements and Gabbott, 2022; Iniesto et al., 2013). Thus, they represent windows of ancient life that can help to unravel the paleoecology, paleobiology and evolution of metazoans, traditionally aided by taphonomic and paleontological studies (Fürsich et al., 2007; Olcott et al., 2022; Varejão et al., 2019). In addition, more robust paleoenvironmental and paleoclimatic context for the exceptional preservation phenomena can help better understand the factors that disrupted the normal organic matter recycling and allowed delicate tissues and remains to become fossils.

La Pedrera de Meià (hereafter LPM), also known as La Pedrera de Rúbies, is a renowned Konservat-Lagerstätte that has provided a huge reference fossil record from the Barremian age, including *Montsechia vidali* (one of the most primitive angiosperm plants, Gómez et al., 2015), *Macryphantes cowdeni* and *Palaeouloborus lacasae* (the most ancient orb-weaver spiders, Selden, 1990), *Meiatermes bertrani* (with two termite castes, one of the most ancient eusocial insect, Martínez-Delclòs and Martinell, 1995) and two different primitive bird taxa, significantly *Noguerornis gonzalezi*, and an unnamed specimen close to *Sulcavis* (Sanz et al., 1997; Chiappe and Lacasa, 2002; Cambra-Moo et al., 2006).

Importantly, the site is also the type locality of 112 holotypes and 19 paratypes of flora and fauna, raising a considerable interest among the scientific community (Galobart et al., 2022; Gil-Delgado et al., 2023). LPM shares similar faunal species with the Las Hoyas Konservat-Lagerstätte (Cuenca, Spain), also of Barremian age (Poyato-Ariza and Buscalioni, 2016), with the common occurrence of arthropods (*Austropotamobius llopisi*, *Delclosia roselli*), insects (*Iderdaegomphus torcae*, *Noguerablatta fontllongae*, *Meiatermes*), fish (*Urocles woodwardi*, *Vidalmia catalaunica*, *Notagogus ferreri*, *Rubiesichthys gregalis*, *Ascalobos*, *Leptolepis*, *Holophagus*), or reptiles (*Meyasaurus*). The plant assemblage includes common species as ferns (*Weichselia reticulata*, *Ruffordia goepperti*, *Sphenopteris*), coniferales (*Frenelopsis rubiesensis*, *Sphenolepis kurriana*), Cycadoposida (*Zamites*) and angiosperms (*Montsechia vidali*). The characterization of the LPM site as a freshwater coastal lake is based on ostracod, insect, and frog assemblages (Brenner et al., 1974; Martínez-Delclòs, 1991; Gómez and Lires, 2019), the charophyte and ranunculacean aquatic flora (Martin-Closas and López-Morón, 1995; Martín-Closas, 2003), together with the total absence of Mesozoic marine fauna. While the site has been the focus of intense paleontological research (Zeiler, 1902; Vidal, 1902; Texeira, 1954; Martínez-Delcòs, 1989; Barale, 1989; Mercadé, 1991; Martínez-Delclòs and Martinell, 1995; Fregenal-Martínez and Meléndez, 1995; Galobart et al., 2022), no detailed analytical work has been performed to assess the lacustrine sedimentary dynamics characterizing these Barremian Lagerstätte deposits. Thus, this study aims at providing a refined multiproxy geochemical-sedimentological framework to shed light on lake paleoenvironmental evolution integrating sedimentary petrography, mineralogy, isotope geochemistry, bulk chemical data, and organic matter content, across a 40 m-thick's well-exposed sedimentary section.

For this reason, the goal of this work is to obtain more quantitative constraints about the paleohydrological, paleoenvironmental and depositional conditions prevailing during the formation of the LPM lithographic limestones.

The remarkable coincidence of LPM site -in terms of microfacies variability, depositional setting, and exceptional fossil preservation- with other renowned Early Cretaceous Lagerstäte deposits like Las Hoyas in Central Spain (Meléndez, 1995; Poyato-Ariza and Buscalioni, 2016; Talbot et al., 1995) constitute a precedent to start applying multidisciplinary approaches to compare and understand these two Konservat-Lagerstätte. Additionally, the present analysis may provide researchers with a refined geochemical methodology for future investigations in similar lagerstätte deposits with limited stratigraphic and/or geochemical resolution (e.g., Solnhofen in Germany; Nusplingen, Causse Méjean, Cerin in France, or Crato in Brazil).

2. Geological setting of the study area

LPM Konservat-Lagerstätte (Fig. 1) is located in the Camarasa and Vilanova de Meià municipalities 875 m-high in the Montsec ranges (Lleida province, NE Spain). These ranges are part of the thrust sheet taking the same name and belonging to the south-Central Pyrenees fold and thrust belt (Séguret, 1972; Muñoz et al., 2018). The studied section is part of a 2000 m thick succession that includes strata from the Triassic to Lower Eocene. The LPM site (see Fig. 1B) is a 40–50 m thick succession of continental mudstones that accumulated in paleolakes on top of the 'Lower Cretaceous unconformity' which resulted from early halokinetic activity (Burrel and Teixell, 2021), and deformed Jurassic carbonates (Fig. 1C). The lateral extension of LPM carbonates is of around 300 m and results from the infill of the small depocenters at the unconformity surface, which was first infilled by Early Cretaceous brecciated carbonates, and subsequently by a Barremian lacustrine lithographic limestone succession (Fig. 1C, in red).

Since its discovery at the end of the 19th century, the LPM Konservat-Lagerstätte has been attributed to different geological ages. In the late 19th and early 20th centuries it was postulated to be Late Jurassic in comparison with the Solnhofen lagoon deposits (Vidal, 1915). In the 70s, based on ostracod associations (Brenner et al., 1974) the unit was dated as Early Cretaceous (Berriasian–Valanginian), and currently, based on charophyte biostratigraphy (Martin-Closas and López-Morón, 1995) the site is considered younger (Early Barremian).

LPM is the most important site, but there are smaller ones located to the East such as La Cabroa, and El Reguer (Fig. 1C). The lacustrine deposits of LPM are known to fill paleotectonic depressions developed on top of a Jurassic–Cretaceous unconformity, with an underlying Lower Cretaceous breccia (see CBeb code, in Pi et al., 2003). As a result of their unique conditions of preservation, they have hosted many discoveries of exquisitely well-preserved fossils from different taxa, including soft tissues, which are not preserved under regular taphonomic conditions. Some of the specimens found include charophytes, fish, and many other vertebrates including frogs, lizards, crocodiles, and birds (Vidal, 1915; Lacasa, 1991; Martínez-Delclòs, 1991, 1995; Lacasa, 2013; Gil-Delgado et al., 2023).

The thickness of the LPM type section ranges between 40 and 50 m (Mercadé, 1991, Gil-Delgado et al., 2023) and is made up of laminated carbonates containing charophytes, ostracods, gastropods, bivalves, and foraminifera. Faunal associations and stratigraphic features enabled the interpretation of environments as formed in quiet, shallow, and well-oxygenated lacustrine settings (Martínez-Delclòs, 1995; Gibert et al., 2000). Moreover, the presence of framboidal pyrite, the sparsity of wave or current sedimentary structures and the exceptional fossil preservation has been interpreted as indicating a relatively stable anoxic lake (Mercadé, 1991).

3. Material and methods

3.1. Material

A total of 303 rock samples were obtained in 3 field campaigns. A first collection of 45 samples spaced at 1 to 2 m intervals was obtained throughout the 50 m-thick section and labeled as "PM", ("Pedrera de Meià"). Another collection of 78 samples very closely spaced (2 to 10 cm interval) was acquired in an interval of 5 m and was named "PR", ("Pedrera de Rúbies"). Finally, a further sampling of 180 levels was undertaken in order to achieve sampling intervals of 25 cm, and was labeled with the acronym "R" ("Rúbies").

Field samples were obtained and powdered with an agate planetary mill.

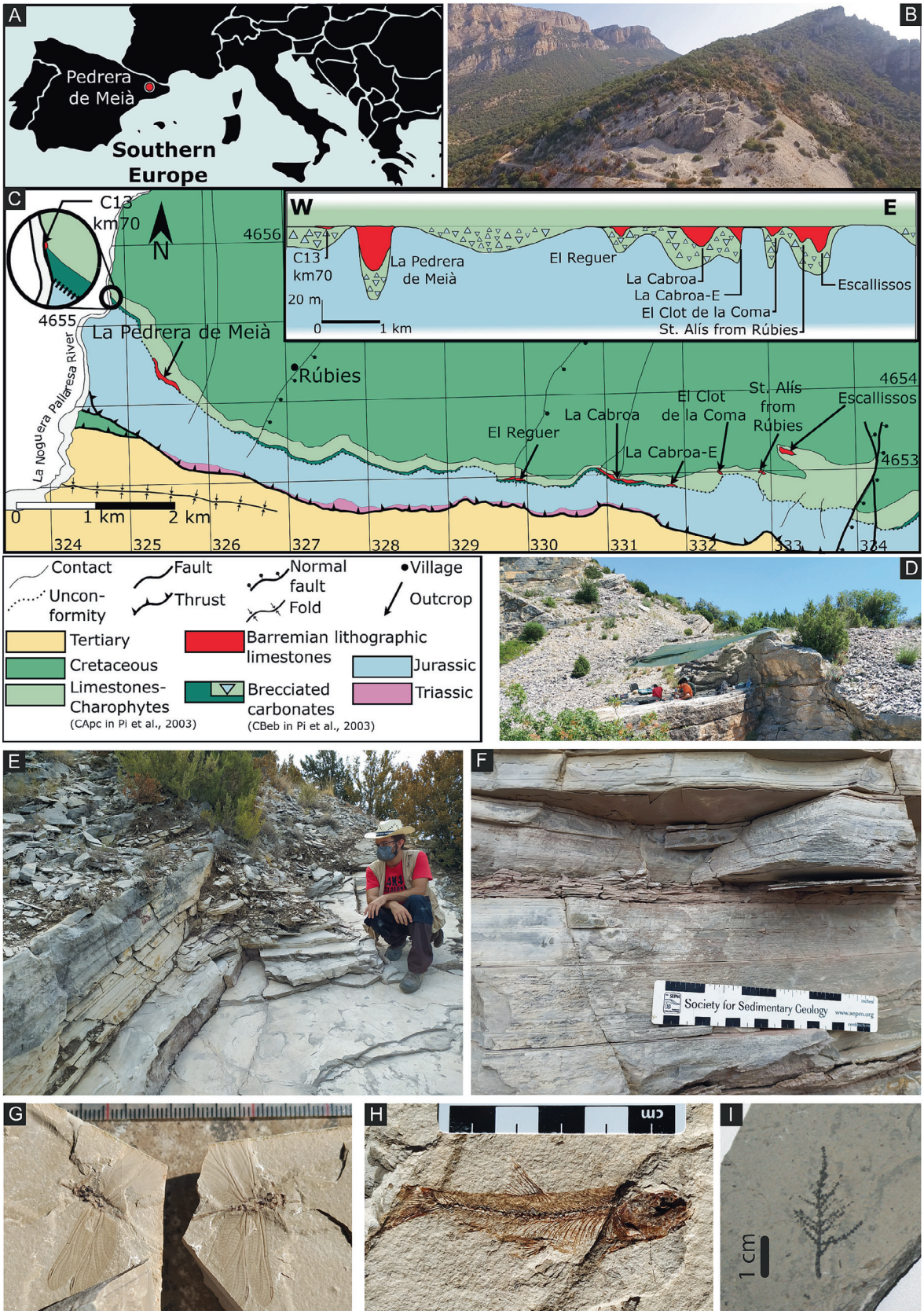

Fig. 1. Location, field views and fossils from the La Pedrera de Meià site (LPM). A). Site's location, B) aerial view of LPM, C) geological map of the Montsec range within the lithographic limestone sites and outcrops in red, the lithographic limestones model section, and legend (modified from Gil-Delgado et al., 2023). D) Image of a field excavation, E) outcrop image of LPM, F) thin-bedded limestones, G) *Ilerdaegomphus*, adult dragonfly, H) a teleostean fish, possibly *Ascalabos* sp. with part of the soft tissues preserved, I) *Montsechia vidalii*.

3.2. Petrography

A microfacies study was carried out on 56 thin sections from throughout the 50 m-thick section (Nikon Eclipse E400 POL). Thin sections were polished with diamond grinding paste to obtain reliable SEM-EDX data (see below).

3.3. Powder X-Ray diffraction (XRD)

Powder X-Ray diffraction was performed throughout the LPM limestones for qualitative and quantitative mineralogical analysis. All samples were carefully powdered and homogenized. XRD measurements were recorded at GEO3BCN-CSIC analytical facilities (Barcelona) by using a Bragg-Brentano diffractometer (Bruker D8-A25) equipped with a LynxEye position sensitive detector. All measurements were acquired with Cu Kα radiation, applying a tube voltage and current of 40 kV and 40 mA, respectively, and using a Ni filter to attenuate Cu Kβ radiation. The scans were typically recorded from 4° to 60° in 2Theta, with a step size of 0.035°, and an equivalent counting time of 192 s per step. Phase identification was carried out with the DIFFRAC.EVA software from Bruker in combination with the Powder Diffraction File PDF-2. Rietveld refinements (Young, 1993) for the calcite phase were carried out by using TOPAS 4.2 software from Bruker. The Rietveld refinements allowed extracting the unit-cell parameters and degree of crystallinity of calcite along the studied succession, thus providing additional proxies to constrain the depositional conditions at LPM.

3.4. Inductively coupled plasma mass spectrometry and X-ray fluorescence

Bulk elemental characterization of LPM section was undertaken with XRF and ICP-MS (see Table S1). XRF analyses were performed on all the samples by using a portable device. The aim of the XRF measurements was to obtain a preliminary semiquantitative estimate of the elemental geochemistry of LPM. For this purpose, the intensity of the relevant XRF peaks was extracted from the spectra (e.g. Ibáñez-Insa et al., 2017). The resulting data was normalized to the intensity of Ca, which allowed an estimate of the relative content along the succession for P, K, Ti, Mn, Fe, Rb and Sr elements among others. The XRF measurements were performed on the same powdered samples used for XRD by using a Bruker Tracer Geo-IV at GEO3BCN-CSIC Barcelona.

In turn, ICP-MS was used to obtain an accurate multi-elemental determination in 46 of the collected samples as wt% (weight percent) of major elements in the form of oxides (e.g. TiO_2, Al_2O_3, Fe_2O_3, etc.) and for minor and trace elements (e.g. Li, Be, Sr, rare-earth elements, etc.) as parts per million (ppm). For this purpose, the powdered samples were analyzed with a Thermo Fisher Scientific Element XR High-Resolution Inductively Coupled Plasma-Mass spectrometer (HR-ICP-MS). The samples were initially dried at 40 °C during 24 h and subsequently acid-digested in closed polytetrafluoroethylene (PTFE) vessels with a combination of HNO_3 + HF + $HClO_4$ (2.5 mL:5 mL:2.5 mL v/v). The samples were then evaporated and, to make a double evaporation, 1 mL of HNO_3 was added to them, which were redissolved and diluted with MilliQ water (18.2 MΩ cm^{-1}) and 1 mL of HNO_3 in a 100 mL volume flask. A tuning solution of 1 μg L^{-1} Li, B, Na, K, Sc, Fe, Co, Cu, Ga, Y, Rh, In, Ba, Tl, U was measured to improve the sensitivity of the ICP-MS, and 20 mg L^{-1} of a monoelemental solution of ^{115}In were added to the samples as internal standard.

The HR-ICP-MS results were employed to determine the Rare-Earth Elements and yttrium elemental concentration (REE + Y) of LPM limestones. The REE + Y contents were normalized to the Post-Archean Australian Shale (PAAS) from McLennan (1989) to obtain elemental anomalies that may provide potential information about lacustrine paleoredox conditions (Ce), marine influence (Y), lake alkalinity (La, Lu, and Gd) and hydrothermal alteration of samples (Eu) (e.g., Möller and Bau, 1993; Bau and Dulski, 1996; Bau et al., 1998; Kim et al., 2012; Tostevin et al., 2016). Additional information about the redox conditions during sedimentation, alkalinity and detrital input was obtained by comparing the Pr/Pr* and Ce/Ce* ratios of samples following the equations of Bau and Dulski (1996) and Lawrence et al. (2006), respectively:

$$Pr/Pr^* = \frac{[Pr]_{SN}}{0.5*[Ce]_{SN} + 0.5*[Nd]_{SN}}$$

$$Ce/Ce^* = \frac{[Ce]_{SN}}{([Pr]_{SN})^2/[Nd]_{SN}}$$

The logCe/Ce* also indicates if LPM carbonates precipitated under oxic or anoxic conditions using the limit of −0.1 established by Elderfield and Pagett (1986), and Wright et al. (1987) as a threshold between both conditions, whereas Y/Ho ratios shed light about the potential influence of seawater (>36), detrital sediment inputs (between 20 and 30) or oxyhydroxides (<25) (Tostevin et al., 2016).

3.5. Scanning electron microscopy-energy dispersive X-ray spectroscopy

Eight thin sections were carbon coated for pyrite framboid analyses using a SEM-EDX at the UAB Microscopy Labs, operating with an acceleration voltage of 20 kV and working with an Oxford Instruments INCA x-Act EVO MA10 software. EDX was used to identify pyrite and other mineralogical estimations. Characterization of pyrite framboids is a potential tool to distinguish between anoxic, dysoxic and oxic conditions in a diversity of depositional environments (Suits and Wilkin, 1998; Wilkin and Barnes, 1997, 1996). Pyrite framboid diameter and characteristics were used to define the following redox categories within LPM limestones (Bond and Wignall, 2010): euxinic conditions (mean 3–5 μm), anoxic conditions (mean 4–6 μm), lower dysoxic conditions (mean 6–10 μm), and oxic conditions (no framboids).

3.6. Loss on ignition

Forty-seven PM samples were prepared for Loss on ignition (LOI) analyses at the GEO3BCN-CSIC labs. LOI is a common method to estimate the organic content in sediments (Heiri et al., 2001) and it is used as an alternative to Total Inorganic Carbon and Total Organic Carbon calculation (TIC and TOC respectively). LOI can be a good approximation and a better tool for many types of samples (Dean, 1974; Dabrio et al., 2004).

3.7. Carbon and oxygen isotope analysis

Carbon and oxygen isotope analyses were performed in continuous flow mode following the procedure described in Breitenbach and Bernasconi (2011), using a GasBench II coupled to a ThermoScientifc MAT 253 mass spectrometer at the ICTA-UAB Stable isotopes Lab (LAIE, Barcelona, Spain). Due to the very low organic content of the original samples, no pre-treatment to remove organics was performed. Between 150 and 400 μg sample powder (homogenized fine fraction), depending on the carbonate content was weighed into borosilicate glass vials and oven-dried at 104 °C overnight. Samples were run at 70 °C for 2.5 h together with international standards NBS19, NBS18, IAEA603 and a working lab standard. All results are reported with respect to the Vienna Pee Dee Belemnite (VPDB) standard. The external standard deviation for oxygen is <0.15 ‰, and for carbon <0.08 ‰.

4. Results

4.1. Sedimentary microfacies

Based on the sedimentary features, texture, and composition of the studied thin sections and outcrops, three sedimentary microfacies have been recognized in the LPM lacustrine succession (Figs. 2 and 3):

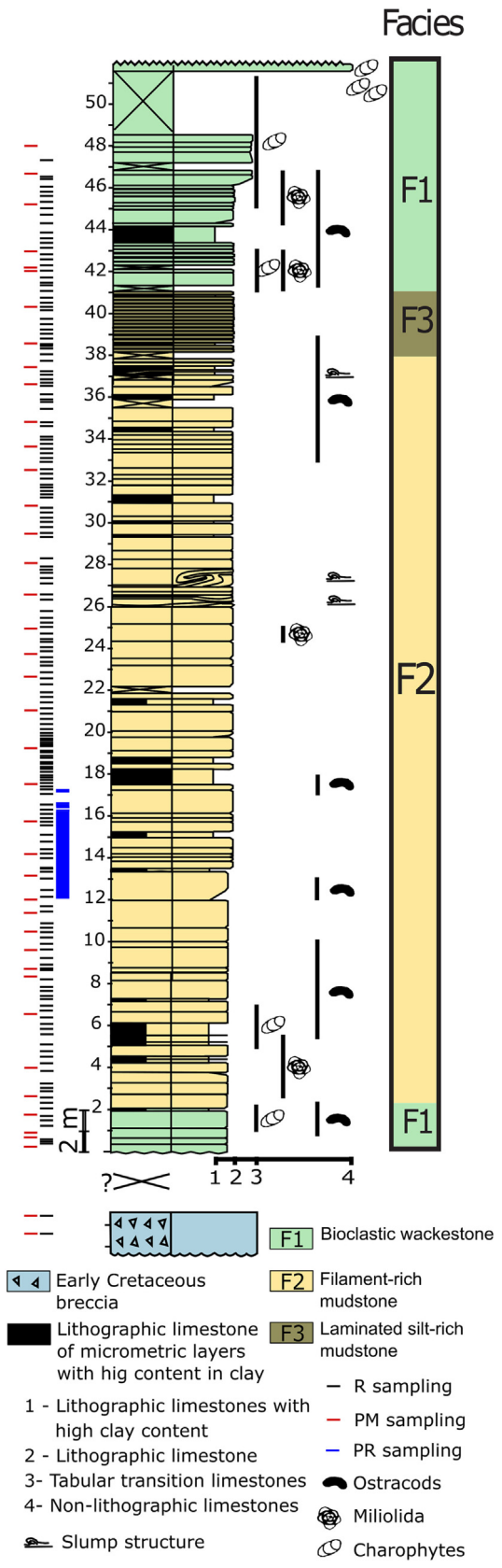

Fig. 2. Sedimentary section of LPM with sampling sites, microfacies types, sedimentary structures, and fossils. See Gil-Delgado et al. (2023) for details.

bioclastic wackestone, Microfacies 1 (F1); microbial filament-rich mudstone, Microfacies 2 (F2); and laminated silt-rich mudstone, Microfacies 3 (F3). Although most of the fossil specimens collected during previous paleontological campaigns were not tied to a specific stratigraphical section, recent surveys show that biota can be found across all the facies in the lithographic limestones section.

4.1.1. Microfacies 1: Bioclastic wackestone

This microfacies is dominant at the base of the section (0 to 2 m), and at the top (41 to 48 m), and occurs as pale gray, tabular and plane parallel beds ranging between 5 and 40 cm in thickness. They are characterized by poorly sorted, organic-rich wackestone to floatstone rich in fragments of charophyte thalli, scarce charophyte gyrogonite debris, freshwater ostracod and brackish miliolid shells, muddy intraclasts, fecal pellets, together with undetermined invertebrate remains (Figs. 2; 3A and B). This microfacies is characterized by relatively variable LOI contents, between 1 and 1.9 % in the first 2 m of the section, and between 0.55 and 1.44 % in the last 7 m. Work in progress indicates that the fossil assemblage from F1 is composed by teleostean fish as *Rubiesichthys gregalis* and *Ascalabos* sp., crustaceans as *Delclosia roselli*, *Montsechia vidalii* remains are very abundant, *Ranunculus* ferreri, *Podozamites* sp., *Brachyphyllum* sp. and some seeds are also recognized in this microfacies; undetermined coprolites are very abundant.

4.1.2. Microfacies 2: Filament-rich mudstone

This microfacies is the most extensive and characterizes the middle part of the LPM sedimentary log, spanning from 2 to 38 m. These limestones display a pale to dark gray color and are organized in plane parallel beds, meter-scale slumped beds (around meter 28), centimetric-scale syn-sedimentary fractures, and centimeter-scale cf. stromatolitic structures. Beds range between 1 and 40 cm in thickness. Petrographically, this microfacies is made up of dark gray to pale brown homogeneous, faintly laminated micrite-rich intervals that occasionally alternate with organic-matter and clastic-rich laminae containing small sand-sized quartz and opaque mineral grains and silt, fragments of fish bones, fine plant debris, and thin-shelled mollusks (Figs. 2 and 3-C and D). Water scape structures and some slumping levels are concentrated in this microfacies, which is distinguished by the conspicuous occurrence of irregularly shaped, contorted filamentous structures that are present as vertically oriented objects (average length of 144.3 μm, $n = 76$; average diameter of 1.06 μm, $n = 13$, Fig. 3D). They occur interspersed in micrite sediment, although some intervals are densely populated by filamentous structures that are accommodated forming dark sub-horizontal laminae. In some samples, fining-upwards millimeter-thick bands are recognized grading from clastic-rich to filament-rich mudstones. Filamentous structures may correspond to sparite crystals with hollow centers as observed in SEM images (Fig. 3D). This microfacies is characterized by variable LOI contents ranging between 2.78 % and 0.66 %, from base to top section. Ongoing research lists fossil assemblages in F2 of fish *Rubiesichthys gregalis*, *Ascalabos* sp., and *Ichthyemidion* sp. among others. The mayfly larvae *Mesopalingea leridae* is very common, and some stratiomyomorphan fly larvae are also found. Plant remains include *Brachyphylum* sp., *Podozamites* sp., *Weichselia?* and some unidentified ferns. Undetermined coprolites are also present.

4.1.3. Microfacies 3: Laminated silt-rich mudstone

This microfacies constitutes the uppermost part of the studied sedimentary section, roughly between 38 and 41 m. These limestones display a pale to dark gray color and are arranged in plane parallel beds ranging between 1 and 20 cm in thickness. They comprise a poorly continuous wavy to irregular laminated texture formed by the alternation of millimeter to sub-millimeter-thick dark gray, organic, and peloidal-rich laminae with pale gray, bioclast and silt-rich laminae in graded intervals (Figs. 2 and 3E-F). Some levels contain thin infilled burrowed

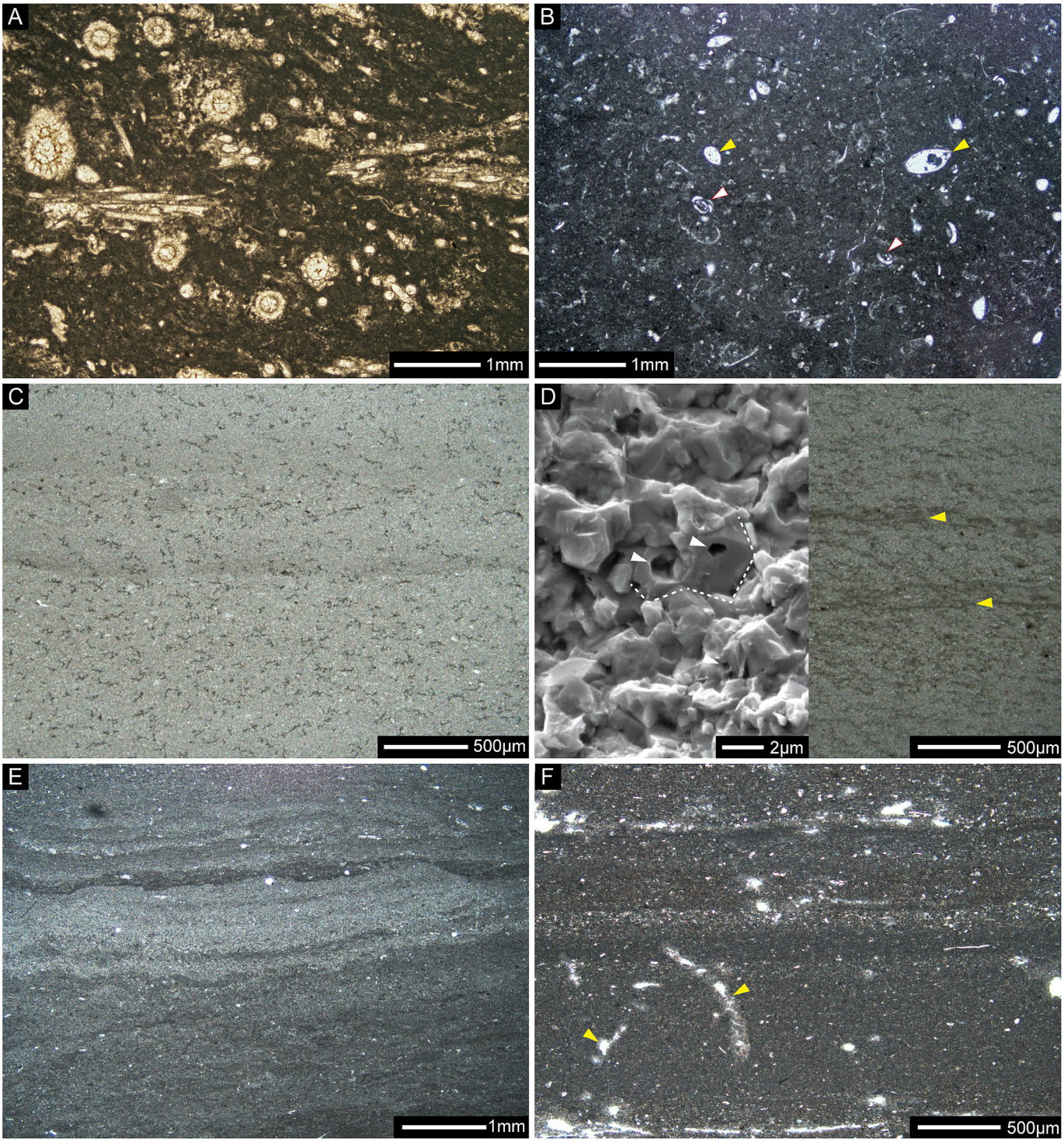

Fig. 3. Microfacies of LPM limestones. A–B) F1: Bioclastic wackestone to floatstone with charophyte thalli, scarce gyrogonite charophyte debris, freshwater ostracod (yellow arrow) and miliolid shell remains (white arrow), intraclasts and fecal pellets. C–D) F2: Filament-rich mudstone constituted by abundant, irregularly shaped, and contorted filamentous structures. Some horizons are densely populated (yellow arrows). SEM photomicrograph of this microfacies showing micrite embedding sparite coatings around hollow centers (white arrows). E–F) F3: Laminated silt-rich mudstone constituted by the alternation of millimeter to sub-millimeter-thick dark gray, organic, and peloidal-rich laminae with pale gray, bioclast and silt-rich laminae in graded intervals. Some thin burrows are observed (yellow arrows).

cavities and poorly sorted intraclasts or bioclastic charophyte remains with intraparticle porosity. Post depositional events are restricted to few small-scale slumps and water scape structures. This microfacies is characterized by variable LOI contents ranging between 2.11 % and 0.38 %, from the base to the top. The paleontological record from this microfacies has not yet been stratigraphically framed.

4.2. Bulk chemical data

The general trends displayed by the most relevant elemental abundancies obtained by ICP-MS are shown in Fig. 4 (seen also Tables S1 and S2). In Fig. 4A (from left to right) titanium (Ti), zirconium (Zr), potassium (K), and aluminum (Al) are grouped. These display a rather

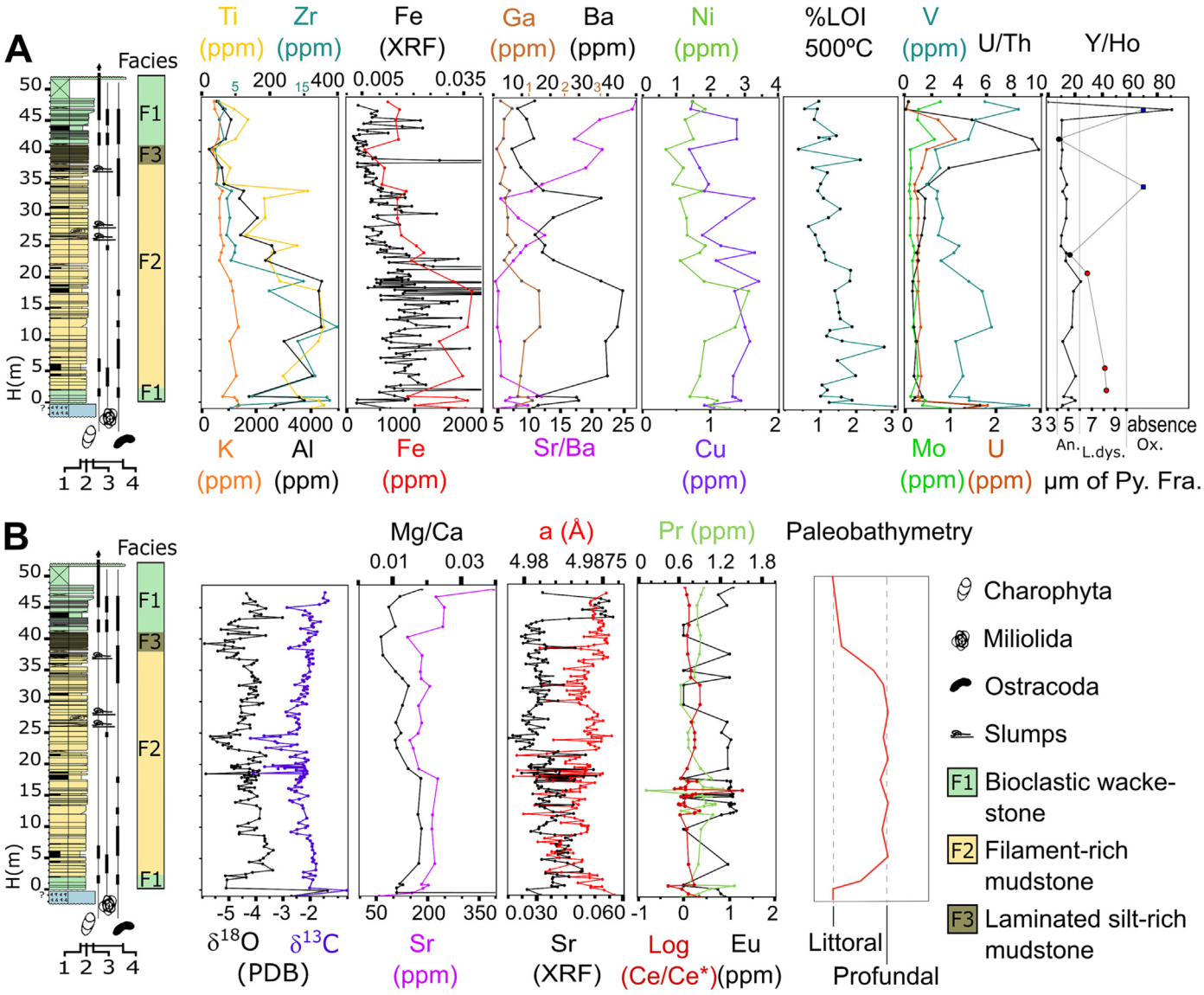

Fig. 4. Summary of geochemical proxies used in this work. A) Combined plot for Ti, Zr, K, and Al as determined from ICP-MS; Fe (ICP-MS vs XRF); Ga, Ba, and Sr/Ba ratio from ICP-MS; Ni, and Cu ICP-MS profiles; Loss on Ignition % (LOI); Mo, U, V, and U/Th ratio from ICP-MS; Y/Ho ratio (ICP-MS), and pyrite framboid diameters categorized as Anoxia (An.), Lower dysoxia (L. dys.) and Oxic zone with no pyrite (Ox.). B) Oxygen ($\delta^{16}O$) and carbon ($\delta^{13}C$) stable isotopes across the succession; Sr and Mg/Ca ratio (ICP-MS); Sr (from XRF) and calcite cell parameter (Rietveld refinement from XRD scans); Pr), log (Ce/Ce*), and Eu anomalies from ICP-MS.

similar decreasing trend (although K is steadier). The very same fashion is observed for iron (Fe), both in the case of the ICP-MS data (ppm values) and that of the more closely spaced XRF results. It is worth mentioning that in the latter case the data are represented with intensity of the Fe Kα peak normalized to that of Ca Kα. As can be seen in Fig. 4, there is good congruence between the two methods. More importantly, the abundance of these elements shows a statistically significant positive correlation (see Figs. S1 and S2, Tables S1 and S2).

Data for gallium (Ga) and barium (Ba) show a decreasing vertical trend as occurs in the case of Fe and for the Ti, Zr, K and Al group (Fig. 4A). In contrast, nickel (Ni) and cupper (Cu) profiles are fairly steady. Loss on Ignition (LOI) displays a smooth decline up section. In addition, molybdenum (Mo), uranium (U) and vanadium (V) reveal stable values from 0 up to 35 m which coincides with a change from microfacies F2 to F3 (Fig. 4A). Above 35 m, an increase for these elements and for the U/Th is identified. In the case of V a saw-shaped profile can be recognized below 35 m. Regarding the Y/Ho ratio, it is found to be steady up to 47 m, while pyrite framboid diameters show a rather decreasing trend up section.

Fig. 4B shows $\delta^{18}O$ and $\delta^{13}C$ carbonate composition across the succession. Both isotopic species seem to exhibit a very similar behavior along the bottom-middle part of the succession (microfacies F1 and F2), and more negative values in the middle part of microfacies F2, and in microfacies F3. Detailed data on carbon and oxygen isotopes is shown in Figs. 5 and 6.

In turn, the Sr and Mg/Ca ratio in Fig. 4 show a similar vertical trend and tend to exhibit increased values up section. This is also reflected in the Sr content as inferred from the XRF intensity of the Kα peak for all the investigated samples, together with the basal lattice parameter of calcite, a (Å), which is expected to reflect the incorporation of impurities in the crystal lattice of the mineral.

Decreased lattice parameters may be linked to the substitutional incorporation of Mg in Ca sites of the crystal structure of calcite (Titschack et al., 2011). Both Sr content and a (Å) show an inverse correlation that is slightly lost from meter 45 onwards (Fig. 4B). It should be noted that

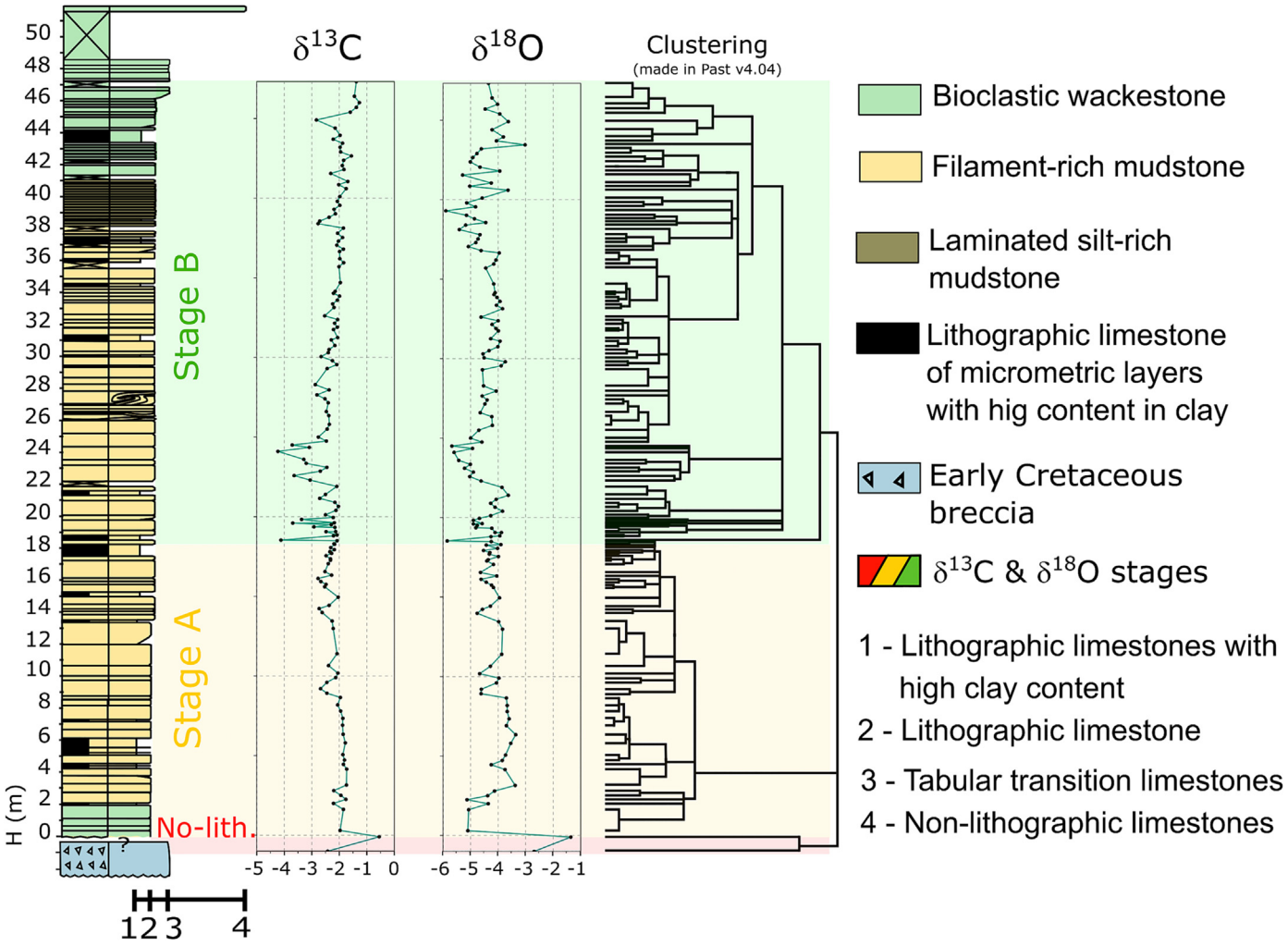

Fig. 5. δ ^{13}C and δ ^{16}O stable isotopes across LPM succession in ‰ VPDB. Data clustering (right) stratigraphically constrained for samples labeled as "R", as obtained with Past software to define 3 zones: No lithographic limestones (No-lith.), stage A and stage B.

Mg cannot be detected with the XRF spectrometer employed in this work. In any case, Mg and Sr as determined by ICP-MS have a positive correlation (see Figs. S1 and S2). The inverse correlation found between Sr (XRF) and cell parameter a (Å) suggests that they are unsuitable to evaluate calcite compositional variations throughout the section (see Figs. S1 and S2).

Finally, profiles for praseodymium (Pr) and log (Ce/Ce*) show a relatively consistent steady trend, while europium (Eu) displays a rather saw-shaped vertical distribution.

The REE + Y contents for the complete carbonate succession results are normalized to the Post-Archean Australian Shale (PAAS) from McLennan (1989) and are shown in Fig. 7. Overall, the patterns for carbonate samples are rather flat (Fig. 7A). Most samples show apparent positive to no Ce anomalies, although very few of them show negative anomalies. The patterns are also characterized by the absence of Eu anomalies, negative to zero Y anomalies, as well as apparent La, Lu and Gd positive anomalies. Additionally, one sample of section top shows a strong Ho negative anomaly.

The Pr/Pr* versus Ce/Ce* cross-plot in (Fig. 7B) shows that most samples display positive Ce anomalies. According to the plot of Ge et al. (2010), which correlates the logCe/Ce* with redox conditions of sedimentation, most of the samples fall within the range of anoxic waters (Fig. 7C).

5. Discussion

5.1. Paleoenvironmental and geochemical reconstruction of LPM Konservat-Lagerstätte succession

5.1.1. Evaluation of the diagenetic overprint

Lacustrine carbonates are sensitive recorders shedding light on depositional conditions, but their textures can be affected by early diagenetic transformations compromising their usefulness for paleoenvironmental reconstructions. Therefore, original signatures must be identified and differentiated from a possible diagenetic overprint. LPM limestones display a set of features supporting a negligible impact of early to burial diagenesis in their textures and geochemical signatures. First, the original laminated fabric is preserved without evidence of recrystallization, neomorphism or cavity filling cements associated with late-stage diagenesis. While some stylolites, and soft-sediment deformation structures (water escape) are observed, they are uncommon and concentrated to specific sedimentary intervals. The occurrence of delicate carbonaceous and filament-rich structures characterizing F2, the abundant and exquisitely well-preserved soft tissues of fossil biota (Martínez-Delclòs, 1991; Gil-Delgado et al., 2023), and the paucity of cementation features or dolomitization textures suggest that late diagenesis was not pervasive. In addition, the anticorrelation between Sr concentrations and calcite lattice parameters

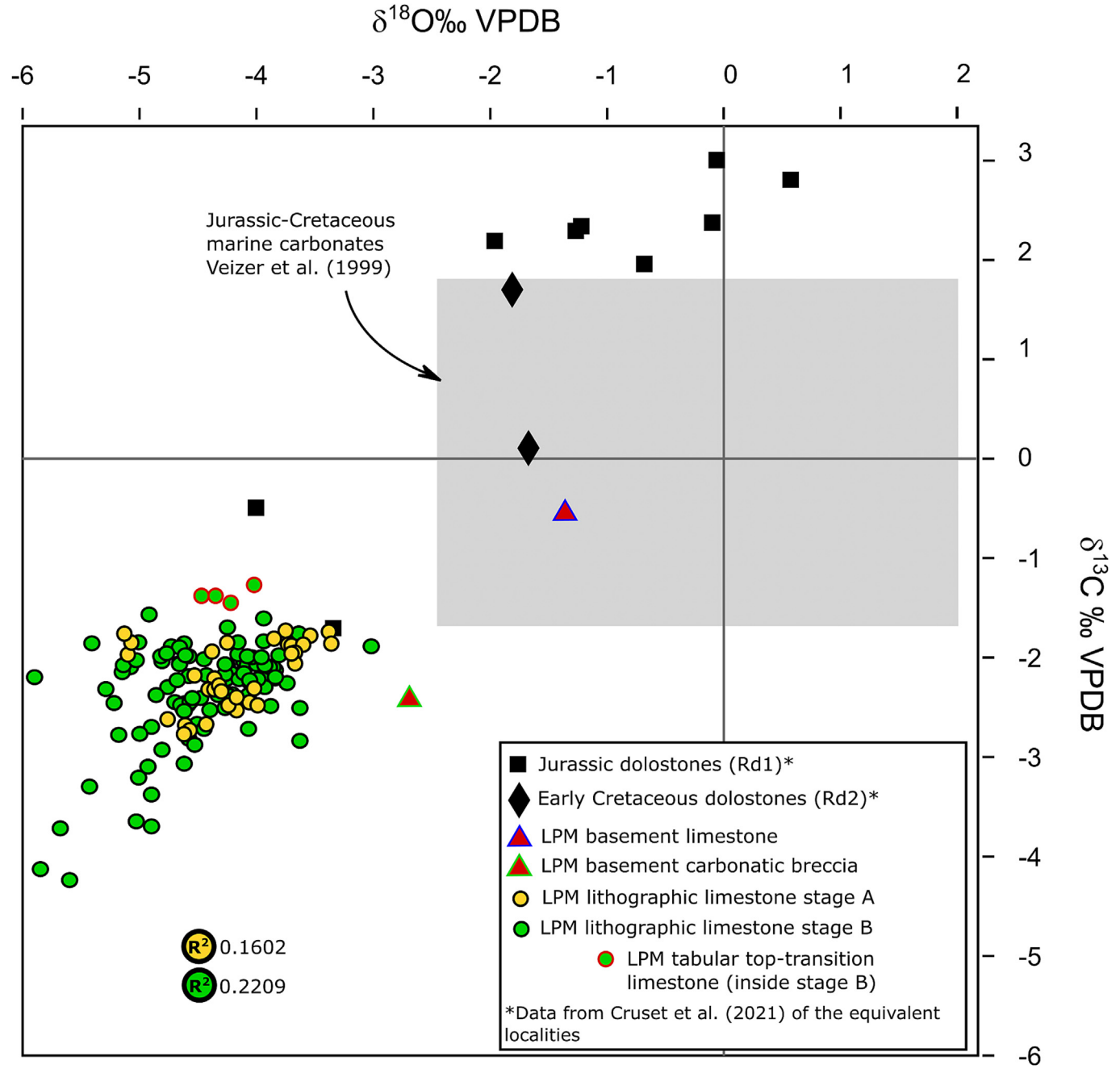

Fig. 6. Cross plot of δ ^{13}C and δ ^{16}O for LPM limestones. Jurassic and Early Cretaceous dolostones from Cruset et al. (2021) are also shown for comparison. Gray rectangle represents the isotopic composition of marine carbonates from Veizer et al. (1999). Yellow circles show samples from stage A of Fig. 5 clustering. Green circles show samples that matches stage B of Fig. 5 clustering. Red triangles represent LPM Mesozoic bedrock signatures.

(see below), and the good correlation between the detrital input proxies and the measured LOI throughout the sedimentary log reflects that LPM limestones (see below) are likely recording quite reliable primary depositional signatures (see Figs. S1 and S2).

5.1.2. Detrital input

In freshwater lakes, sedimentary profiles of Al, K, Fe and Ti trace elements can be commonly associated with terrestrial sediment discharge into the lake reflecting the mineralogical by-products of soil weathering (Cohen, 2003; Kylander et al., 2011; Moreno et al., 2007; Rohais et al., 2019; Tribovillard et al., 2006; Wintsch and Kvale, 1994). Thus, these elements can be used for reconstructions of detrital input either as fluvial or eolian contributions aided by their low mobility during diagenesis (Gomes et al., 2020; Wintsch and Kvale, 1994) Therefore, the decreasing concentration of Al, Ti, and K throughout the LPM succession and their strong correlation with Fe points to a reduced input of terrigenous fractions up section probably associated with a lessening of freshwater ingress into the lake (Cohen, 2003; Davison, 1993) (Fig. 4A). The vertical profile of Zr and Rb (not shown) also points to decreased enrichment in fine-grained clay material from the middle of the section onwards. However, it should be noted that the presence of silt and sand-sized quartz grains is moderately sparse but homogenous across the studied microfacies from petrographic observations. XRD and XRF analyses confirm a very minor but steady contribution of siliceous materials and/or clay to the calcareous mudstones which is also supported by absence of negative Ce anomalies (Rieger et al., 2022).

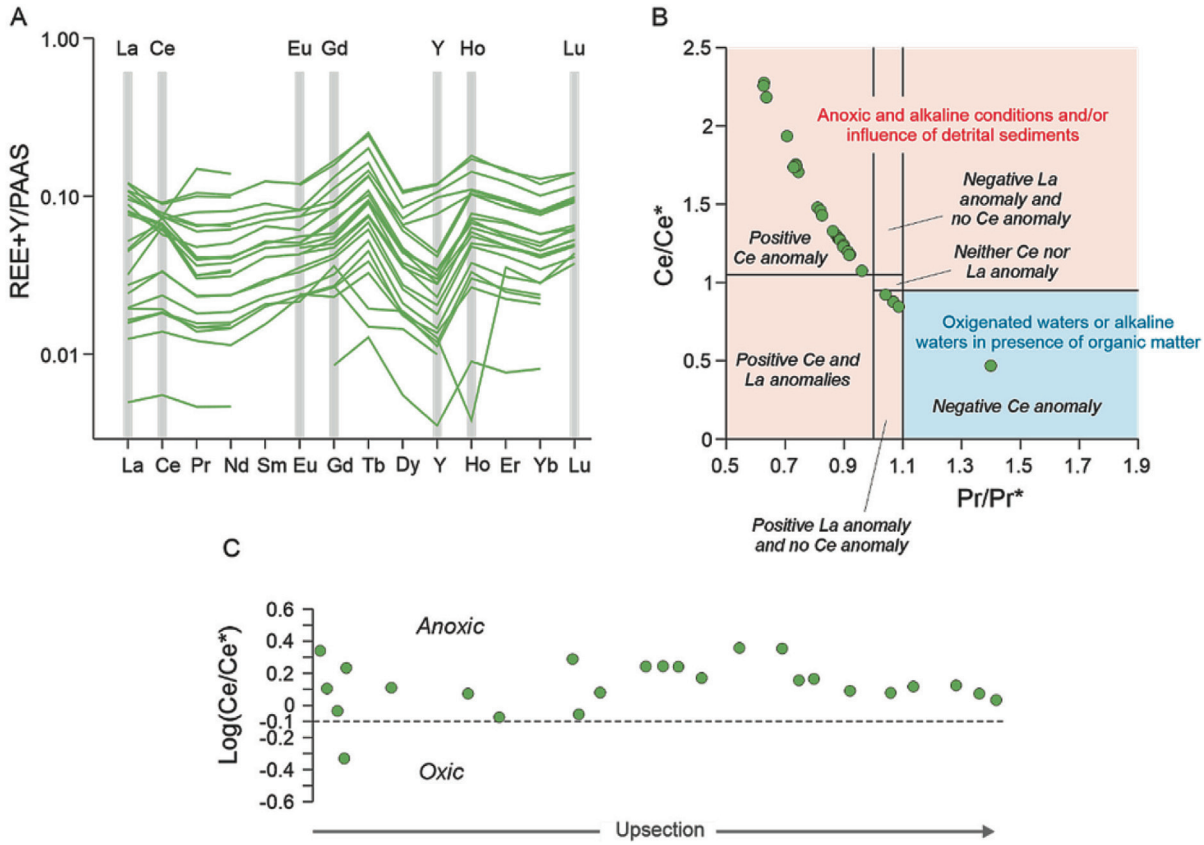

Fig. 7. A–B) PAAS-normalized REE + Y distribution patterns of carbonates of the LPM. C) PAAS-normalized Ce/Ce* versus Pr/Pr* cross-plot to analyze the Ce and Pr anomalies of carbonate samples. The method of Bau and Dulski (1996) modified by Webb and Kamber (2000) was used. D) Log(Ce/Ce*) of carbonate samples. The distinction between oxic and anoxic conditions at −0.10 is based on Elderfield and Pagett (1986) and Wright et al. (1987).

5.1.3. Paleosalinity and evaporation trends

LPM limestones have been commonly described as having formed in extensive coastal lakes that evolved in close connection to the continent (Gibert et al., 2000). While fossil associations collectively suggest deposition in a non-marine lacustrine environment such as charophytes, ostracods, mayfly and dragonfly nymphs, frogs, etc., (Gibert et al., 2000; Martínez-Delclòs, 1995), punctuated marine ingressions could have occurred. The scarce but recurrent presence of miliolid foraminifera in F1 (either in the lowermost and uppermost part of the section) may indicate periods of saltier conditions developed in shallow freshwater lakes that evolve to coastal brackish lakes (Anadon, 1989; Pérez-Cano et al., 2022). Brackish waters are generated mainly through a spatially heterogeneous mixing of freshwater and seawater which can be affected by seasonal evaporation increases (Anadón et al., 2002; Mackenzie et al., 1995; Rosen et al., 1996), so disentangling the origin of salinity departures in ancient lacustrine successions is challenging. To estimate potential salinity fluctuations throughout LPM lake system, Ga, Ba, Sr, and Sr/Ba elemental concentrations in mudstones were analyzed (Fig. 4). Gallium is primarily derived from weathering processes on quartzose and feldspathic silicate rocks, and, due to strong particulate scavenging, Ga concentrations in seawater are usually lower than in freshwater systems (Wei and Algeo, 2020). In the same way, Ba provenance in mudstones can be associated with the weathering reactions of naturally occurring Ba-rich catchment minerals: i.e., barite ($BaSO_4$) or witherite ($BaCO_3$), since crustal concentrations are very low (Wei and Algeo, 2020; Wolgemuth and Broecker, 1970). For this reason, Ba contents in freshwaters tend to be much higher than in marine waters (Wolgemuth and Broecker, 1970). Therefore, Ga and Ba might be potentially used as tracers of freshwater contributions to lake systems when compared with the abundances of Sr (Wei and Algeo, 2020). In LPM mudstones, strong correlations exist between the patterns of Ga and Ba, and those observed for Al, Fe and Zr, suggesting that Ga and Ba might have entered the lake through metal remobilization from weathering of catchment lithologies (see Figs. S1 and S2). If this assumption is correct, the increased inputs of Ba and Ga to the lake must have been more prominent throughout the first half of the section and have declined from the second half to the top, which is consistent with the overall reduction of the detrital input up section. Strontium could also derive from the chemical weathering of Sr-rich catchment minerals (i.e., plagioclase, gypsum, calcite, dolomite, celestine or strontianite); however, a relatively constant abundance of Sr (between 150 and 250 ppm) is observed in LPM mudstones. In addition, a very poor statistical significance with detrital-associated elements such as Al, Fe, Zr, K and Ti has been recognized pointing toward an alternative source of Sr other than limestone catchment weathering (see Figs. S1 and S2). Since Sr average concentrations in seawater are ~105 times greater compared to those in freshwater (Wei and Algeo, 2020), a marine-derived contribution of Sr could be plausible in a coastal lacustrine setting. Collectively, the Sr/Ba ratio has been employed as a successful proxy to identify salinity fluctuations in mudrocks (Wei and Algeo, 2020) and organic-rich lacustrine deposits (Fathy et al., 2021; Li et al., 2020). In this respect, LPM limestones show unusually high Sr/Ba values (from 10 to 25) at the topmost part of the section coincident with a change in depositional character from F2 to F3 going up section, and also with the occurrence of some miliolids (Fig. 4A). However, the REE + Y signatures of LPM limestones show negative to zero Y anomalies and apparent La, Lu and Gd anomalies, which could discard a persistent marine influence during lacustrine deposition (Bau et al., 1998). Increased salinity could also be attributed to enhanced evaporation in shallower coastal-lake environments which could leave a geochemical signature in $\delta^{18}O$. While more positive $\delta^{18}O$ values are correlated with the highest Sr/Ba values observed, it is difficult to ascertain whether

this is related to increased evaporation or to a decline in continental freshwater circulation (Ingram et al., 1996). Additional work would be required to better assess the nature of salinity fluctuations in LPM coastal-lacustrine succession (e.g., Sr isotopes).

5.1.4. Paleoproductivity

Primary productivity in lake systems can be very high but the concentrations of organic matter in lacustrine sediments only record a fraction of the total biological production in surface waters. Thus, increases in primary production in ancient lacustrine successions can be associated with fluctuations of the organic debris that escapes dissolution, heterotrophic organism degradation or bacterial decay (Cohen, 2003; Lerman, 1978; Tribovillard et al., 2006). Despite these complications, the delivery of organic matter of the sediment-water interface and the final burial flux can be considered proportional to surface-water productivity (Gierwsloski-Kordesch, 2010; Tribovillard et al., 2006). LPM samples contain a conspicuous abundance of organic remains including fragments of fish bones, clotted dark patches intermingled in charophyte floatstones, and an abundant assemblage of filament-rich mudstones suggesting a considerable lake productivity. In addition, LOI values recorded in the different microfacies point to a decreasing concentration of organic matter up section. Such a decline could be associated with either an apparent reduction in organic productivity in younger sedimentary environments, or to a decreased preservation potential due to fluctuating redox conditions in the sediments. Moreover, Ni and Cu are increasingly used as paleoproductivity proxies in different lake and marine systems as these elements can be easily scavenged by organic matter and dominantly delivered to the sediments (Li et al., 2020; Rohais et al., 2019; Tribovillard et al., 2006). In line with this, the good correlation between Ni or Cu and LOI reinforces the idea that relatively high contents of Ni and Cu in LPM lacustrine sediments could indicate a high flux of organic matter delivery to the basin (Figs. 4, S1 and S2). Interestingly, good correlations between Ni and Cu with Al, Fe, Ti, and K, might suggest that detrital fluxes to the lake correlate well with primary productivity peaks as has been previously proposed in other lacustrine basins (Wang et al., 2017) (see Figs. S1 and S2).

5.1.5. Paleoxygenation-redox conditions

Redox-sensitive trace proxies (V, U, Mo, U/Th ratios) have been extensively used as paleoredox indicators in ancient sedimentary systems (Bennett and Canfield, 2020; Tribovillard et al., 2012, 2006; Wang et al., 2017). Their usefulness is based on the fluctuations in the solubility and redox state tied to specific chemical conditions at the time of sediment deposition (water-sediment interface) or during early diagenesis within sediment pore waters. Thus, the patterns of trace metal enrichment into authigenic minerals and sediments have proven valuable tools to discriminate between oxic, dysoxic, or anoxic conditions (Jones and Manning, 1994; Rohais et al., 2019; Tribovillard et al., 2006). In LPM samples a particular enrichment in the concentrations of U (1.12 ppm, V (8.32 ppm), and Mo (0.66 ppm) is recognized in the uppermost part of the succession (between 40 and 47 m) suggesting enhanced oxygen depletion above the transition between F3 to F1 (Fig. 4). A possible explanation for the higher U and Mo enrichments compared with lower and flatter values in F2 (mean of 0,4 μg/g and 0,2 μg/g, respectively) could be attributed to either: i) higher water renewal rates from adjacent water bodies (freshwater or marine) supplying dissolved U and Mo to the lake, or ii) higher organic carbon fluxes associated to biologically-derived particulates in the water column which are enriched in non-lithogenic U or Mo (Bennett and Canfield, 2020; Tribovillard et al., 2006; Wagner et al., 2017). Furthermore, the peak in redox-sensitive trace metals coincides with a peak in organic productivity (LOI) and a remarkable change from F2 to F3. This microfacies shift could be attributed to a variation in the identity of the primary producers and carbonate production potential, which in turn could have modified the depositional rates increasing the uptake of uranyl and Mo complexes into LPM mudstone sediments (Bennett and Canfield, 2020; Tribovillard et al., 2006). In line with this, the particularly lower and flatter values of U and Mo for most of the lower and middle parts of the succession could be explained as a result of a hydrographically restricted lake water circulation which could have limited the accumulation of these trace metals in deep-water sediments favoring dysoxic to anoxic bottom conditions (Bennett and Canfield, 2020; Tribovillard et al., 2006). A restricted water circulation during the early stages of LPM lacustrine sedimentation is also proposed here based on the observed covariance in the carbon and oxygen isotopic trends (see discussion below). While V has been also commonly employed for paleo-redox inferences (Jones and Manning, 1994; Rohais et al., 2019), the broad patterns in V geochemistry across the LPM succession show a different behavior to that of U and Mo (Fig. 4). The heterogeneous saw-shaped profile in V concentrations from the first half of the succession could be attributed to fluctuations in the Mn—Fe cycling typical during reducing conditions which can modify the adsorption of V onto Fe—Mn oxyhydroxides (Tribovillard et al., 2006), and carbonate sediments (Cohen, 2003; Hild and Brumsack, 1998). In such reducing conditions, a high solubility of Mn^{2+} in sediments may have resulted in Mn being heterogeneously depleted in LPM mudstones. Additional evidence supporting suboxic conditions during LPM deposition is provided by the systematic study of pyrite framboid size distribution in the different facies (Suits and Wilkin, 1998; Wilkin et al., 1996; Wilkin and Barnes, 1997). The lower part of LPM succession shows mean pyrite framboids between 8.10 and 8.28 μm, the middle portion exhibits framboid diameters between 5.12 and 6.76 μm, while the upper section contains mean framboids of 4.18 μm. Collectively, these data suggest the predominance of dysoxic conditions in the first half of the succession, and a wider redox behavior (from anoxic to oxygenic conditions) in the second half and toward the upper part of LPM section. Moreover, the REE + Y contents show that the absence of negative Ce anomalies (Fig. 7A and B) could also indicate lacustrine sedimentation under anoxic conditions (Rieger et al., 2022) confirming the overall trend.

5.1.6. Paleohydrology

The $\delta^{18}O$ composition of all the mudstone samples ranges between about −3 ‰, and −6 ‰, and therefore differs significantly from Late Barremian–Early Aptian marine signatures (Veizer et al., 1999; Wissler et al., 2003) (Figs. 4 to 6). In addition, a non-marine or coastal terrestrial setting is supported by the lighter $\delta^{13}C$ values (between −1 ‰ and −4 ‰) typically recorded in these environments (Heimhofer et al., 2010; Paz and Rossetti, 2006) compared to marine equivalents which range from +2 ‰ to +4 ‰ (Veizer et al., 1999; Wissler et al., 2003). Similar negative oxygen isotope values have been interpreted to belong to continental freshwater settings in the geological record (Camoin et al., 1997; Gallois et al., 2018; Paz and Rossetti, 2006; Talbot, 1990) although marine-influenced continental environments might exhibit lighter values (Ingram et al., 1996).

The balance between influx and evaporation is responsible of drastic changes in lake isotopic composition (Horton et al., 2016; Li and Ku, 1997; Talbot, 1990) which in turn has been associated to fluctuations in lake levels and climate (Camoin et al., 1997; Heimhofer et al., 2010; Paz and Rossetti, 2006). Trends in $\delta^{18}O$ composition suggest that LPM mudstones can be subdivided in two stages: i) a lowermost stage A (from 2 m to 18 m) showing a paucity in isotopic variability (between −5 ‰ and −3,5 ‰); and ii) an uppermost stage B (from 18 m to 45 m) with more frequent and wider variabilities (between −6 ‰ and −3 ‰). The data from the first interval could represent intermittent perturbations in lake levels with evaporative (^{18}O-rich values) and freshwater input (^{16}O-rich values) events of similar magnitude (Fig. 5). Conversely, the uppermost interval seems to show rapid and wider fluctuations in the hydrological cycle as also demonstrated by the reduced input

of terrigenous fractions, a possible marine contribution to the lake, and/or combined with enhanced evaporation.

Moreover, inorganic carbon isotope signatures of LPM limestones might have fluctuated according to different processes. The dissolution of the Jurassic-Cretaceous catchment limestones (with $\delta^{13}C$ between −0.5 ‰ and −2.5 ‰) may have had an influence on the carbon isotopic composition of the groundwaters inflowing to the lake explaining, at least in part, the −1 ‰ to −4 ‰ carbon isotopic values of LPM limestones (Leng and Marshall, 2004). A progressive change in biological productivity and carbonate factories (between F2 and F3) could have a significant impact of the $\delta^{13}C$ of the dissolved inorganic carbon (DIC) pool of LPM lake. Preferred uptake of ^{12}C by aquatic photoautotrophic organisms (including charophytes and other littoral plants) would lead to a progressive depletion of the carbon pool and enrichment of ^{13}C, as is observed in LPM carbonates across the uppermost stage B (Giorgio, 2005; Kelts and Talbot, 1990).

Finally, the modest positive covariance between the carbon and oxygen isotope curves of LPM limestones (with correlation coefficients of 0.16 in stage A, and 0.22 in stage B) may be interpreted as possible deposition in hydrologically closed to semi-closed basins (Cohen, 2003; Kelts and Talbot, 1990; Li and Ku, 1997; Talbot, 1990) (Figs. 5 and 6). The temporal oscillations in oxygen and DIC isotopic compositions suggest LPM waterbodies having relatively long residence times and more frequent water level fluctuations.

5.2. Carbonate production modes and LPM depositional evolution

The analysis of microfacies and depositional textures indicates the predominance of two main carbonate sources in LPM sedimentary succession: i) biogenic calcareous shells, and ii) chemically and biologically mediated precipitation of authigenic carbonate minerals. In one side, F1 is dominated by a carbonate factory including charophyte remains (thalli and gyrogonites), ostracods, thin-shelled bivalves, and some miliolids embedded in fine-grained, organic-rich mudstones (Fig. 8). This biotic association is typically encountered in littoral areas of the lake margins characterized by low-energy, shallow-water, and oxygenated depositional environments colonized by aquatic photosynthetic organisms that may disintegrate forming carbonate muds (Kelts and Hsü, 1978; Platt and Wright, 1991; Valero-Garcés et al., 2014). On the other hand, the formation of the filament-rich mudstones (F2) constituted by micrite embedding sparite coatings around hollow centers could have involved in situ precipitation of micrite mediated by picocyanobacteria inhabiting the lake (Dittrich and Obst, 2004), combined with chemical precipitation due to increased evaporation or lake water temperature changes (Gierwsloski-Kordesch, 2010; Kelts and Talbot, 1990; Valero-Garcés et al., 2014; Verrecchia, 2002). The complete lack of bioturbation and faintly laminated and homogeneous texture of this microfacies suggest deposition under low-energy, calm and deeper conditions (Fig. 4). Although changes in filament density and lateral arrangement are observed in some micrite intervals, it is challenging to decipher the reasons for such a distribution. However, it is plausible to consider seasonal fluctuations in water chemistry, intensity of detrital events, redox conditions, or nutrient load as factors influencing the occurrence and preservation of the filamentous structures in these profundal sediments. Since most of the sedimentary succession in LPM Konservat-Lagerstäte is constituted by F2, future work is warranted to better characterize the potential geomicrobiological roles that might be associated with the exceptional preservation of LPM fossil assemblages (Clements and Gabbott, 2022; Varejão et al., 2019). Finally, the depositional texture and sedimentary characteristics of F3 suggest sedimentation in a moderate to low energy lacustrine setting episodically sourced by carbonate mud and silt-sized particles (Fig. 8). The occurrence of tiny burrow cavities, scour surfaces and bioclastic components collectively suggest deposition in shallower, more oxygenated, and agitated environments than those forming F3 (Fig. 4). In summary, the vertical distribution of microfacies and sedimentological observations suggest an early lake flooding event (F2 on top of F1) followed by a progressive shallowing (F1 on top of F3) which is also supported by the distribution of terrigenous fractions up-section (see Section 5.1.2), and the change in carbonate factories (see Figs. 4 and 8).

Moreover, the calcite mineralogy identified in LPM limestones may have resulted from an originally low Mg/Ca ratio of the Barremian lake waters or porewaters (Chagas et al., 2016; Kelts and Hsü, 1978; Müller et al., 1972). The fact that Sr and Mg/Ca ratios of calcites are running in parallel in the first half of the LPM succession probably attest that fluctuations in solution stoichiometry affected the incorporation of Mg and Sr into calcite (Nehrke et al., 2007; Nielsen et al., 2013), as reflected in the lattice parameters of calcite. However, such co-dependency is less remarkable in the uppermost part of the section probably indicating: i) a change in the calcifying mechanisms from non-skeletal muds (F2–F3) to charophyte calcification (F1); or ii) a diagenetic modification of the original mineralogies at the transition between the two carbonate factories. Furthermore, it is interesting to note the strong anticorrelation between Sr and calcite lattice spacings, suggesting that mineralization patterns are affected by the pathways of Sr and/or Mg incorporation into calcite (Wasylenki et al., 2005) (see Figs. S1 and S2).

6. Conclusions

The limestones of La Pedrera de Meià (LPM) in south-Central Pyrenees provide one of the best-preserved successions of lacustrine-coastal Barremian lagerstätte in Europe. This multiproxy study represents an attempt to reconstruct the depositional environments and

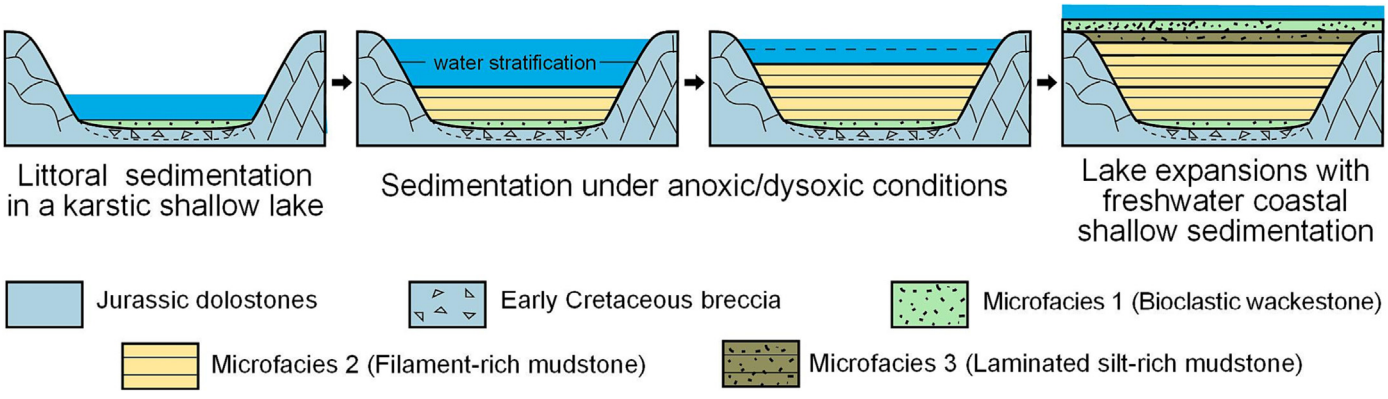

Fig. 8. Diagram showing the lacustrine sedimentary evolution and microfacies distributions of LPM from left to right. Shallow-water lacustrine carbonates (microfacies F1) characterized the first stage of the depositional evolution. Progressive deepening of the lake gave rise to deposition of profundal microfacies F2 under anoxic to dysoxic conditions, followed by deposition of microfacies F3 in shallower, more oxygenated, and agitated environments. The late stage is constituted by the deposition of shallow water carbonates (microfacies F1) in a coastal-lacustrine environment.

paleoenvironmental fluctuations associated to this unique Konservat-Lagerstätte. Combining sedimentological and geochemical data several conclusions can be drawn:

1. LPM succession documents an overall evolution of a coastal lake showing a transition from profundal to littoral lacustrine environments both recording the exceptional preservation of fossil biotic assemblages. Littoral settings are characterized by low/moderate-energy, shallow-water, and oxygenated conditions where charophytes, ostracods and miliolids accumulated in mud-rich facies (microfacies F1). Profundal facies are made up of filament-rich mudstones (microfacies F2) originated from in situ precipitation of micritic sediments either biotically mediated or physico-chemically induced and deposited in virtually undisturbed, low-energy environments under anoxic conditions. While the biota that lived in the oxygenated areas of the lake is preserved, the terrestrial biota has been shed by flotation or by slow currents.
2. The analysis of stable $\delta^{13}C$ and $\delta^{18}O$ and redox-sensitive geochemical elements (V, Mo, U, U/Th, REE + Y) points to deposition in a hydrologically closed to semi-closed lacustrine basin with a restricted water circulation (water stratification) favoring dysoxic to anoxic conditions in profundal sediments. These conditions were prevalent during the entire deposition of LPM carbonates playing a key role in the exceptional preservation of the biotas.
3. Paleoproductivity proxies (Ni, Cu, LOI) suggest that terrestrial sediment discharge to the lake correlate well with primary productivity peaks. In addition, a decline in terrigenous input to the lake (fine-grained clastic fraction) is here interpreted because of the progressive reduction of meteoric water entrance at the upper part of the succession. These trends are also supported by the Ba and Ga signatures in LPM carbonates which points to reduced catchment weathering up section.
4. Whereas different lines of evidence advocate a salinity increase toward the younger lake deposits (Sr/Ba ratios, presence of miliolids, isotopic signatures), it is difficult to determine whether this is related to increased evaporation, or to a combination of reduced continental freshwater circulation to the lake, or to sporadic seawater inputs to the lake.

The present study provides a framework to decode the paleohydrological and paleoenvironmental fluctuations in similar lithographic limestones worldwide. A straightforward application of this methodology could be the case of the renowned lagerstätte deposits from Las Hoyas in central Spain (Meléndez, 1995; Poyato-Ariza and Buscalioni, 2016; Talbot et al., 1995).

Additional targets might include other outstanding lithographic limestone sites such as Solnhofen and Nusplingen in Germany, Causse Méjean and Cerin in France, or Crato in Brazil. According to our results the multiproxy study of these sites would benefit from a closely spacing geochemical sampling on the basis of ICP-MS, REE analysis, calcite cell parameter, organic matter content, and stable isotope data. Future studies in LPM will improve the proxies' database by including Sr stable isotopes, biomarker signatures, or evaluating the possible involvement of microbial processes in biota preservation. Interestingly, the multiproxy framework presented may enable to precisely locate fossil specimens in the section by analyzing their host-rock geochemical signature. Finally, an integrated taphonomic study may be developed by considering the depositional model and the abiotic and biotic processes that appear to influence the exceptional preservation phenomena.

CRediT authorship contribution statement

AGD: Conceptualization, Methodology, Software, Validation, Formal analysis, Investigation, Data curation, Writing - original draft, Visualization. **DC**: Software, Writing - original draft, Formal Analysis. **OO**: Conceptualization, Methodology, Formal analysis, Resources, Writing - original draft, Supervision, Project administration, Funding acquisition. **EB**: Formal analysis, Investigation; **JI**: Methodology, Software, Validation, Formal analysis, Investigation; **XD**: Funding acquisition, investigation, review; **AS**: Investigation, review; **AG**: investigation, Project Administration, review; **RMM**: Conceptualization, Validation, Methodology, Formal analysis, Investigation, Writing - original draft, review & editing, Visualization, Funding acquisition.

Data availability

Data will be made available on request.

Declaration of competing interest

The authors declare the following financial interests/personal relationships which may be considered as potential competing interests: Alejandro Gil-Delgado reports financial support was provided by Autonomous University of Barcelona. Alejandro Gil-Delgado reports administrative support was provided by Museu de la Conca Dellà. Alejandro Gil-Delgado reports financial support was provided by International Association of Sedimentologists. David Cruset reports financial support was provided by Geosciences Barcelona. Ramon Mercedes-Martin reports financial support was provided by Autonomous University of Barcelona. Xavier Delclos reports financial support was provided by University of Barcelona. Jordi Ibanez-Insa reports financial support was provided by Geosciences Barcelona. Albert Selles reports administrative support was provided by Museu de la Conca Dellà. Angel Galobart reports administrative support was provided by Museu de la Conca Dellà. Oriol Oms reports financial support was provided by Autonomous University of Barcelona.

Acknowledgements

This work has been funded by Spanish Government MCIN project PGC2018-101575-B-I00. "Dynamics of transitional settings from Cretaceous to Eocene in the south central Pyrenees"; and the Generalitat de Catalunya (CERCA Program). AGD was supported by the AGAUR program for the doctoral formation grant 2020 FI SDUR 00360. ASG research is supported by the project VIGEOCULT (PLEC2021-00793) funded by MCIN/AEI/10.13039/501100011033 and by the European Union NextGenerationEU/PRTR. ASG and AG acknowledges the project ARQ001SOL-173-2022 ("El Cretaci continental del Pirineu meridional català: ecosistemes I evolució faunística. 2022-2025") funded by the Departament de Cultura of the Generalitat de Catalunya and the CERCA Program. We are indebted to Vilanova the Meià and Camarasa local authorities, as well as Orígens UNESCO Global Geopark to facilitate fieldwork in the Montsec area. AGD benefited from an International Association of Sedimentologists IAS Postgraduate Grant to cover field work and geochemical expenses. This work is part of the PhD Thesis of AGD (made in the framework of a PhD Doctoral Programme in Geology at UAB), and EB Undergraduate Thesis project. We would like to thank Soledad Alvarez (GEO3BCN-CSIC) for technical support with the XRD and XRF measurements. The constructive and detailed comments by Prof. Giorgio Basilici and an anonymous reviewer contributed to sharpen the manuscript and are kindly acknowledged.

Appendix A. Supplementary data

Supplementary data to this article can be found online at https://doi.org/10.1016/j.sedgeo.2023.106440.

References

Anadon, P., 1989. Los lagos salinos interiores (atalásicos) con faunas de afinidad marina del Cenozoico de la Península Ibérica. Acta Geologica Hispánica 24 (2), 83–102.

Anadón, P., Gliozzi, E., Mazzini, I., 2002. Paleoenvironmental reconstruction of marginal marine environments from combined paleoecological and geochemical analyses on

ostracods. In: Holmes, Chivas (Ed.), The Ostracoda: Applications in Quaternary Research https://doi.org/10.1029/gm131.
Barale, G., 1989. Sur trois geo espèces de coniférales du Crétacé Inférieur "Espagne". Intérêts paléoécologiques et stratigraphiques. Review of Palaeobotany and Palynology 62, 303–318.
Bau, M., Dulski, P., 1996. Distribution of yttrium and rare-earth elements in the Penge and Kuruman iron-formations, Transvaal Supergroup, South Africa. Precambrian Research 79, 37–55. https://doi.org/10.1016/0301-9268(95)00087-9.
Bau, M., Usui, A., Pracejus, B., Mita, N., Kanai, Y., Irber, W., Dulski, P., 1998. Geochemistry of low-temperature water–rock interaction: evidence from natural waters, andesite, and iron-oxyhydroxide precipitates at Nishiki-numa iron-spring, Hokkaido, Japan. Chemical Geology 151, 293–307. https://doi.org/10.1016/S0009-2541(98)00086-2.
Bennett, W.W., Canfield, D.E., 2020. Redox-sensitive trace metals as paleoredox proxies: a review and analysis of data from modern sediments. Earth Science Reviews 204, 103175. https://doi.org/10.1016/j.earscirev.2020.103175.
Bond, D.P.G., Wignall, P.B., 2010. Pyrite framboid study of marine Permian–Triassic boundary sections: a complex anoxic event and its relationship to contemporaneous mass extinction. GSA Bulletin 122, 1265–1279. https://doi.org/10.1130/b30042.1.
Breitenbach, S.F., Bernasconi, S.M., 2011. Carbon and oxygen isotope analysis of small carbonate samples (20 to 100 μg) with a GasBench II preparation device. Rapid Communications in Mass Spectrometry 25 (13), 1910–1914.
Brenner, P., Geldmacher, W., Schroedeer, R., 1974. Ostrakoden und Alter der Plattenkalke von Rubies (sierra del Montsech, Prov. Lérida, NE Spanien). Neues Jahruch für Geologie und Paläontologie 9, 513–524.
Burrel, L., Teixell, A., 2021. Contractional salt tectonics role of pre-existing diapiric structures in the Southern Pyrenean foreland fols-thrust belt (Montsec and Serres Marginals). Journal of the Geological Society 2020–2085.
Cambra-Moo, O., Chamero, B., Marugán-Lobón, J., Delclòs, X., Poyato-Ariza, F.J., Buscalioni, A.D., 2006. Estimating the ontogenetic status of an enantiornithine bird from the Lower Barremian of El Montsec, Central Pyrenees, Spain. Estudios Geológicos 62 (1), 241–248.
Camoin, G., Casanova, J., Rouchy, J.M., Blanc-Valleron, M.M., Deconinck, J.F., 1997. Environmental controls on perennial and ephemeral carbonate lakes: the central palaeo-Andean Basin of Bolivia during Late Cretaceous to early Tertiary times. Sedimentary Geology 113, 1–26. https://doi.org/10.1016/s0037-0738(97)00052-3.
Chagas, A.A.P., Webb, G.E., Burne, R.V., Southam, G., 2016. Modern lacustrine microbialites: towards a synthesis of aqueous and carbonate geochemistry and mineralogy. Earth-Science Reviews 162, 338–363. https://doi.org/10.1016/j.earscirev.2016.09.012.
Chiappe, L., Lacasa, A., 2002. Noguernis gonzalei (Aves: Ornithothoraces) from the Early Cretaceous of Spain. In: Witmer (Ed.), Mesozoic Birds: Above the Heads of Dinosaurs Chiappe. University of California Press, pp. 230–239.
Clements, T., Gabbott, S., 2022. Exceptional preservation of fossil soft tissues. eLS 2, 1–10. https://doi.org/10.1002/9780470015902.a0029468.
Cohen, A.S., 2003. Paleolimnology the History and Evolution of Lake Systems. Oxford geo Press.
Cruset, D., Vergés, J., Benedicto, A., Gómez-Rivas, E., Cantarero, I., John, C.M., Travé, A., 2021. Multiple fluid flow events from salt-related rifting to basin inversion (Upper Pedraforca thrust sheet, SE Pyrenees). Basin Research 33 (6), 3102–3136.
Dabrio, C.J., Santisteban, J.I., Mediavilla, R., Lo, E., Castan, S., Zapata, M.B.R., Jose, M., 2004. Loss on ignition: a qualitative or quantitative method for organic matter and carbonate mineral content in sediments? Journal of Paleolimnology 32, 287–299.
Davison, W., 1993. Iron and manganese in lakes. Earth-Science Reviews 34, 119–163. https://doi.org/10.1016/0012-8252(93)90029-7.
Dean, W.E., 1974. Determination of Carbonate and Organic Matter in calcareous sediments and sedimentary rocks by loss on ignition: comparison with other methods. Journal of Sedimentary Petrology 44 (I), 242–248.
Dittrich, M., Obst, M., 2004. Are picoplankton responsible for calcite precipitation in lakes? Ambio: A Journal of the Human Environment 33 (8), 559–564.
Elderfield, H., Pagett, R., 1986. Rare earth elements in ichthyoliths: variations with redox conditions and depositional environment. Science of the Total Environment 49, 175–197. https://doi.org/10.1016/0048-9697(86)90239-1.
Fathy, D., Wagreich, M., Ntaflos, T., Sami, M., 2021. Paleoclimatic variability in the southern Tethys, Egypt: insights from the mineralogy and geochemistry of Upper Cretaceous lacustrine organic-rich deposits. Cretaceous Research 126, 104880. https://doi.org/10.1016/j.cretres.2021.104880.
Fregenal-Martínez, M., Meléndez, N., 1995. Geological setting in Montsec & Montral-Alcover, Two Konservat-Lagerstätten, Catalonia, Spain. In: Martínez-Delclòs, X. (Ed.), Field Trip Guidebook. II International Symposium on Lithographic Limestones, pp. 12–23.
Fürsich, F.T., Werner, W., Schneider, S., Mäuser, M., 2007. Sedimentology, taphonomy, and palaeoecology of a laminated plattenkalk from the Kimmeridgian of the northern Franconian Alb (southern Germany). Palaeogeography, Palaeoclimatology, Palaeoecology 243, 92–117. https://doi.org/10.1016/j.palaeo.2006.07.007.
Galobart, À., Párraga, J., Gil-Delgado, A., 2022. The spread of fossil heritage: how to valorise the lithographic limestones of the La Pedrera de Meià and La Cabroa Quarries in the Orígens Unesco Global Geopark (Southern Pyrenees, Catalonia). Geoheritage 14, 34. https://doi.org/10.1007/s12371-022-00669-w.
Gallois, A., Bosence, D., Burgess, P.M., 2018. Brackish to hypersaline facies in lacustrine carbonates: Purbeck Limestone Group, Upper Jurassic–Lower Cretaceous, Wessex Basin, Dorset, UK. Facies 64, 1–39.
Ge, L., Jiang, S.-Y., Swennen, R., Yang, T., Yang, J.-H., Wu, N.-Y., Liu, J., Chen, D.H., 2010. Chemical environment of cold seep carbonate formation on the northern continental slope of South China Sea: evidence from trace and rare earth element geochemistry. Marine Geology 277, 21–30.
Gibert, J.M. de, Fregenal-Martínez, M.A., Buatois, L.A., Mángano, M.G., 2000. Trace fossils and their palaeoecological significance in Lower Cretaceous lacustrine conservation deposits, El Montsec, Spain. Palaeogeography, Palaeoclimatology, Palaeoecology 156, 89–101. https://doi.org/10.1016/s0031-0182(99)00133-9.
Gierwsloski-Kordesch, 2010. Carbonate Lacustrine Settings, Facies, Environments. Developments in SedimentologyVolume 61.
Gil-Delgado, A., Delclòs, X., Sellés, A., Galobart, À., Oms, O., 2023. The Early Cretaceous coastal lake Konservat-Lagerstätte of La Pedrera de Meià (Southern Pyrenees). Geologica Acta 21.3 (1-18), I–XIII. https://doi.org/10.1344/GeologicaActa2023.21.3.
Giorgio, D., 2005. Respiration in aquatic ecosystems. Limnology and Oceanography Bulletin 14, 74–76. https://doi.org/10.1002/lob.200514474.
Gomes, J.P., Bunevich, R.B., Tedeschi, L.R., Tucker, M.E., Whitaker, F.F., 2020. Facies classification and patterns of lacustrine carbonate deposition of the Barra Velha Formation, Santos Basin, Brazilian Pre-salt. Marine and Petroleum Geology 113, 104176. https://doi.org/10.1016/j.marpetgeo.2019.104176.
Gómez, R.O., Lires, A.I., 2019. High ecomorphological diversity among Early Cretaceous frogs from a large subtropical wetland of Iberia. Comptes Rendus Palevol 18 (7), 711–723.
Gómez, B., Daviero-Gómez, V., Coiffard, C., Martín-Closas, C., Dilcher, D.L., 2015. Montsechia, an ancient aquatic angiosperm. Proceedings of the National Academy of Sciences 112 (35), 10985–10988.
Heimhofer, U., Ariztegui, D., Lenniger, M., Hesselbo, S.P., Martill, D.M., Rios-Netto, A.M., 2010. Deciphering the depositional environment of the laminated Crato fossil beds (Early Cretaceous, Araripe Basin, North-eastern Brazil). Sedimentology 57, 677–694. https://doi.org/10.1111/j.1365-3091.2009.01114.x.
Heiri, O., Lotter, A.F., Lemcke, G., 2001. Loss on ignition as a method for estimating organic and carbonate content in sediments: reproducibility and comparability of results. Journal of Paleolimnology 25 (1), 101–110. https://doi.org/10.1023/A:1008119611481.
Hild, E., Brumsack, H.J., 1998. Major and minor element geochemistry of Lower Aptian sediments from the NW German Basin (core Hohenegglesen KB 40). Cretaceous Research 19, 615–633. https://doi.org/10.1006/cres.1998.0122.
Horton, T.W., Defliese, W.F., Tripati, A.K., Oze, C., 2016. Evaporation induced ^{18}O and ^{13}C enrichment in lake systems: a global perspective on hydrologic balance effects. Quaternary Science Reviews 131, 365–379. https://doi.org/10.1016/j.quascirev.2015.06.030.
Ibáñez-Insa, J., Pérez-Cano, J., Fondevilla, V., Oms, O., Rejas, M., Fernández-Turiel, J.L., Anadón, P., 2017. Portable X-ray fluorescence identification of the Cretaceous–Paleogene boundary: application to the Agost and Caravaca sections, SE Spain. Cretaceous Research 78, 139–148.
Ingram, B.L., Conrad, M.E., Ingle, J.C., 1996. Stable isotope and salinity systematics in estuarine waters and carbonates: San Francisco Bay. Geochimica et Cosmochimica Acta 60, 455–467. https://doi.org/10.1016/0016-7037(95)00398-3.
Iniesto, M., Lopez-Archilla, A.I., Fregenal-Martinez, M., Buscalioni, A.D., Guerrero, M.C., 2013. Involvement of microbial mats in delayed decay: an experimental essay on fish preservation. Palaios 28 (1), 56–66.
Jones, B., Manning, D.A., 1994. Comparison of geochemical indices used for the interpretation of palaeoredox conditions in ancient mudstones. Chemical Geology 111 (1–4), 111–129.
Kelts, K., Hsü, K.J., 1978. Freshwater carbonate sedimentation. Lakes: Chemistry, Geology, Physics, pp. 295–323 https://doi.org/10.1007/978-1-4757-1152-3_9.
Kelts, Talbot, 1990. Lacustrine carbonates as geochemical archives of environmental change and biotic-abiotic.pdf. Large Lakes: Ecological Structure and Function, pp. 288–315.
Kim, J.H., Torres, M.E., Haley, B.A., Kastner, M., Pohlman, J.W., Riedel, M., Lee, Y.J., 2012. The effect of diagenesis and fluid migration on rare earth element distribution in pore fluids of the northern Cascadia accretionary margin. Chemical Geology 291, 152–165.
Kylander, M.E., Ampel, L., Wohlfarth, B., Veres, D., 2011. High-resolution X-ray fluorescence core scanning analysis of Les Echets (France) sedimentary sequence: new insights from chemical proxies. Journal of Quaternary Science 26, 109–117. https://doi.org/10.1002/jqs.1438.
Lacasa, A., 1991. Els jaciments fossilífers de les calcàries litogràfiques del Montsec. In: Martínez-Delclòs, X. (Ed.), Les calcàries litogràfiques del Cretaci inferior del Montsec. Deu anys de campanyes paleontològiques. I.E.I, pp. 15–19.
Lacasa, A., 2013. Resumen histórico sobre la edad de los yacimientos de calizas litográficas del Montsec. Batalleria 18, 41–44.
Lawrence, M.G., Creig, A., Collerson, K.D., Kamber, B.S., 2006. Rare earth element and yttrium variability in Southeast Queensland Waterways. Aquatic Geochemistry 12, 39–72. https://doi.org/10.1007/s1049 8-005-4471-8.
Leng, M.J., Marshall, J.D., 2004. Palaeoclimate interpretation of stable isotope data from lake sediment archives. Quaternary Science Reviews 23, 811–831. https://doi.org/10.1016/j.quascirev.2003.06.012.
Lerman, A., 1978. Lakes, Chemistry, Geology, Physics. Springer-Verlag, Berlin https://doi.org/10.1007/978-1-4757-1152-3.
Li, H.-C., Ku, T.-L., 1997. d13C– d18C covariance as a paleohydrological indicator for closed-basin lakes. Palaeogeography Palaeoclimate Palaeoecolecology 133, 69–80. https://doi.org/10.1016/s0031-0182(96)00153-8.
Li, Q., Wu, S., Xia, D., You, X., Zhang, H., Lu, H., 2020. Major and trace element geochemistry of the lacustrine organic-rich shales from the Upper Triassic Chang 7 Member in the southwestern Ordos Basin, China: implications for paleoenvironment and organic matter accumulation. Marine and Petroleum Geology 111, 852–867. https://doi.org/10.1016/j.marpetgeo.2019.09.003.
Mackenzie, F.T., Vink, S., Wollast, R., Chou, L., 1995. Comparative geochemistry of marine saline lakes. Physics and Chemistry of Lakes. 265–278. https://doi.org/10.1007/978-3-642-85132-2_9.

Martín-Closas, C., 2003. The fossil record and evolution of freshwater plants: a review. Geologica Acta 1 (4), 315–338.
Martin-Closas, C., López-Morón, N., 1995. Systematic paleontology. In: Martínez-Delclòs, X. (Ed.), Montsec and Mont-ral-Alcover, Two Konservat-Lagerstätten. Catalonia. Spain. International II Symposium on Lithographic Limestones. Field Trip Guide Book. Institut d'Estudis Ilerdencs, pp. 29–61.
Martínez-Delclòs, X., 1991. Les Calcàries Litogràfiques del Cretaci Inferior del Montsec. Deu Anys de Campanyes Paleontològiques. Institut Estudis Ilerdencs 84-87029-22-1.
Martínez-Delclòs, X., 1995. Montsec and Montral-Alcover, two Konservat-lagerstätten, Catalonia, Spain. II International Symposium on Lithographic Limestones. Field Trip Guide Book, July 9-11st.
Martínez-Delclòs, X., Martinell, J., 1995. The oldest known record of social insects. Journal of Paleontology 69 (3), 594–599.
Martínez-Delcòs, X., 1989. Chresmoda aquatica insecto chresmodidae del Cretácico inferior de la Sierra del Montsec, España. Revista Espanola de Paleontologia 4, 67–74.
McLennan, S., 1989. Rare earth elements in sedimentary rocks; influence of provenance and sedimentary processes. Reviews in Mineralogy and Geochemistry 21, 277–290.
Meléndez, N., 1995. Las Hoyas: A Lacustrine Konservat-Lagerstätte, Cuenca, Spain. Editorial Complutense, Madrid.
Mercadé, Ll, 1991. Context geològic. Sedimentologia de les calcàries litogràfiques del Cretaci inferior de la serra del Montsec (Espanya). In: Martínez-Delclós, X. (Ed.), The Lower Cretaceous Lithographic Limestones of Montsec. Ten Years of Paleontological Expeditions. Institut Estudis Ilerdencs, Lleida, Spain.
Möller, P., Bau, M., 1993. Rare-earth patterns with positive cerium anomaly in alkaline waters from Lake Van, Turkey. Earth and Planetary Science Letters 117, 671–676. https://doi.org/10.1016/0012-821X(93)90110-U.
Moreno, A., Giralt, S., Valero-Garcés, B., Sáez, A., Bao, R., Prego, R., Pueyo, J.J., González-Sampériz, P., Taberner, C., 2007. A 14kyr record of the tropical Andes: the Lago Chungará sequence (18°S, northern Chilean Altiplano). Quaternary International 161, 4–21. https://doi.org/10.1016/j.quaint.2006.10.020.
Müller, G., Irion, G., Förstner, U., 1972. Formation and diagenesis of inorganic Ca–Mg carbonates in the lacustrine environment. Naturwissenschaften 59, 158–164. https://doi.org/10.1007/bf00637354.
Muñoz, J.A., Mencos, J., Roca, E., Carrera, N., Gratacós, O., Ferrer, O., Fernández, O., 2018. The structure of the South-Central-Pyrenean fold and thrust belt as constrained by subsurface data. Geologica Acta 16 (4), 439–460. https://doi.org/10.1344/GeologicaActa2018.16.4.7.
Nehrke, G., Reichart, G.J., Cappellen, P.V., Meile, C., Bijma, J., 2007. Dependence of calcite growth rate and Sr partitioning on solution stoichiometry: non-Kossel crystal growth. Geochimica et Cosmochimica Acta 71, 2240–2249. https://doi.org/10.1016/j.gca.2007.02.002.
Nielsen, L.C., Yoreo, J.J.D., DePaolo, D.J., 2013. General model for calcite growth kinetics in the presence of impurity ions. Geochimica et Cosmochimica Acta 115, 100–114. https://doi.org/10.1016/j.gca.2013.04.001.
Olcott, A.N., Downen, M.R., Schiffbauer, J.D., Selden, P.A., 2022. The exceptional preservation of Aix-en-Provence spider fossils could have been facilitated by diatoms. Communications Earth and Environment 3, 94. https://doi.org/10.1038/s43247-022-00424-7.
Paz, J.D.S., Rossetti, D.F., 2006. Paleohydrology of an Upper Aptian lacustrine system from northeastern Brazil: integration of facies and isotopic geochemistry. Palaeogeography Palaeoclimate Palaeoecology 241, 247–266. https://doi.org/10.1016/j.palaeo.2006.03.040.
Pérez-Cano, J., Bover-Arnal, T., Martín-Closas, C., 2022. Charophyte communities in Barremian Iberian wetlands. Facies 68, 13. https://doi.org/10.1007/s10347-022-00651-6.
Pi, E., Colomer, M., Samsó, J.M., Caus, E., Arbués, P., Cuevas, J.L., Barberà, X., Corregidor, J., Escuer, J., Solà, J., Montaner, J., Berástegui, X., 2003. Mapa geològic de Catalunya. 1: 25000. Llimiana 290–1-2 (65–24). Institut Cartogràfic de Catalunya.
Platt, N.H., Wright, V.P., 1991. Lacustrine Facies Analysis. pp. 57–74 https://doi.org/10.1002/9781444303919.ch3.
Poyato-Ariza, F.J., Buscalioni, A., 2016. Las Hoyas: A Cretaceous Wetland: A Multidisciplinary Synthesis After 25 Years of Research on an Exceptional Fossil Lagerstätte From Spain. Friedrich Verlag (260pp., DOI: 9783899371536).
Rieger, P., Magnall, J.M., Gleeson, S.A., Oelze, M., Wilke, F.D., Lilly, R., 2022. Differentiating between hydrothermal and diagenetic carbonate using rare earth element and yttrium (REE+ Y) geochemistry: a case study from the Paleoproterozoic George Fisher massive sulfide Zn deposit, Mount Isa, Australia. Mineralium Deposita 57 (2), 187–206.
Rohais, S., Hamon, Y., Deschamps, R., Beaumont, V., Gasparrini, M., Pillot, D., Romero-Sarmiento, M.F., 2019. Patterns of organic carbon enrichment in a lacustrine system across the K-T boundary: insight from a multi-proxy analysis of the Yacoraite Formation, Salta rift basin, Argentina. International Journal of Coal Geology 210, 103208. https://doi.org/10.1016/j.coal.2019.05.015.
Rosen, M.R., Coshell, L., Turner, J.V., Woodbury, R.J., 1996. Hydrochemistry and nutrient cycling in Yalgorup National Park, Western Australia. Journal of Hydrology 185, 241–274. https://doi.org/10.1016/0022-1694(95)02981-8.
Sanz, et al., 1997. A nestling bird from the Lower Cretaceous of Spain: implications for avian skull and neck evolution. Science 276, 1543–1546.
Séguret, M., 1972. Etude tectonique des nappes et gs décollées de la partie centrale du vessant sud des Pyrénées. Caractère synsédimentaire, rôle de la geo et de la gravité. (PhD Thesis)Laboratoire de géologie geo-USTL, Montpellier.
Selden, P., 1990. Lower Cretaceous spiders from the Sierra de Montsech, North-East Spain. Palaeontology 33 (2), 257–285.
Suits, N.S., Wilkin, R.T., 1998. Pyrite formation in the water column and sediments of a meromictic lake. Geology 26, 1099–1102. https://doi.org/10.1130/0091-7613(1998)026<;1099:pfitwc>2.3.co;2.
Talbot, M.R., 1990. A review of the palaeohydrological interpretation of carbon and oxygen isotopic ratios in primary lacustrine carbonates. Chemical Geology: Isotope Geoscience Section 80, 261–279. https://doi.org/10.1016/0168-9622(90)90009-2.
Talbot, M.R., Meléndez, N., Fregenal-Martínez, M.A., 1995. The waters of the Las Hoyas lake: sources and limnological characteristics. In: Meléndez, N. (Ed.), Las Hoyas, pp. 11–16.
Texeira, C., 1954. La flore des calcaires lithographiques de Meya (Lerida, Espagne). Boletin da Sociedad Geologica de Portugal 11, 139–151.
Titschack, J., Goetz-Neunhoeffer, F., Neubauer, J., 2011. Magnesium quantification in calcites [$(Ca,Mg)CO_3$] by Rietveld-based XRD analysis: revisiting a well-established method. American Mineralogist 96 (7), 1028–1038. https://doi.org/10.2138/am.2011.3665.
Tostevin, R., Shields, G.A., Tarbuck, G.M., He, T., Clarckson, M.O., Wood, R.A., 2016. Effective use of cerium anomalies as a redox proxy in carbonate-dominated marine settings. Chemical Geology 438, 146–162. https://doi.org/10.1016/j.chemg eo.2016.06.027.
Tribovillard, N., Algeo, T.J., Lyons, T., Riboulleau, A., 2006. Trace metals as paleoredox and paleoproductivity proxies: an update. Chemical Geology 232, 12–32. https://doi.org/10.1016/j.chemgeo.2006.02.012.
Tribovillard, N., Algeo, T.J., Baudin, F., Riboulleau, A., 2012. Analysis of marine environmental conditions based on molybdenum–uranium covariation—applications to Mesozoic paleoceanography. Chemical Geology 324, 46–58. https://doi.org/10.1016/j.chemgeo.2011.09.009.
Valero-Garcés, B., Morellón, M., Moreno, A., Corella, J.P., Martín-Puertas, C., Barreiro, F., Pérez, A., Giralt, S., Mata-Campo, M.P., 2014. Lacustrine carbonates of Iberian Karst Lakes: sources, processes and depositional environments. Sedimentary Geology 299, 1–29. https://doi.org/10.1016/j.sedgeo.2013.10.007.
Varejão, F.G., Warren, L.V., Simões, M.G., Fürsich, F.T., Matos, S.A., Assine, M.L., 2019. Exceptional preservation of soft tissues by microbial entombment: insights into the taphonomy of the Crato Konservat-Lagerstätte. Palaios 34 (7), 331–348.
Veizer, J., Ala, D., Azmy, K., Bruckschen, P., Buhl, D., Bruhn, F., Carden, G.A.F., Diener, A., Ebneth, S., Godderis, Y., Jasper, T., Korte, C., Pawellek, F., Podlaha, O.G., Strauss, H., 1999. 87Sr/86Sr, d13C and d18O evolution of Phanerozoic seawater. Chemical Geology 161, 59–88. https://doi.org/10.1016/s0009-2541(99)00081-9.
Verrecchia, E.P., 2002. Lacustrine and palustrine geochemical sediments. Journal of Paleolimnology 27, 221–237. https://doi.org/10.1023/a:1014263722766.
Vidal, L.M., 1902. Nota sobre la presencia del tramo Kimeridgense en el Montsech (Lerida) y hallazgo de un batracio en sus hiladas. Memorias de la Real Academia de Ciencias y Artes de Barcelona 1–12 (3)4(18).
Vidal, L.M., 1915. Nota geológica y paleontológica sobre el Jurásico superior de la provincia de Lérida. Boletín. Instituto Geológico y Minero de España 36, 1–43.
Wagner, M., Chappaz, A., Lyons, T.W., 2017. Molybdenum speciation and burial pathway in weakly sulfidic environments: insights from XAFS. Geochimica et Cosmochimica Acta 206, 18–29. https://doi.org/10.1016/j.gca.2017.02.018.
Wang, C., Wang, Q., Chen, G., He, L., Xu, Y., Chen, L., Chen, D., 2017. Petrographic and geochemical characteristics of the lacustrine black shales from the Upper Triassic Yanchang Formation of the Ordos Basin, China: implications for the organic matter accumulation. Marine and Petroleum Geology 86, 52–65. https://doi.org/10.1016/j.marpetgeo.2017.05.016.
Wasylenki, L.E., Dove, P.M., Wilson, D.S., Yoreo, J.J.D., 2005. Nanoscale effects of strontium on calcite growth: an in situ AFM study in the absence of vital effects. Geochimica et Cosmochimica Acta 69, 3017–3027. https://doi.org/10.1016/j.gca.2004.12.019.
Webb, G.E., Kamber, B.S., 2000. Rare earth elements in Holocene reefal microbialites: a new shallow seawater proxy. Geochimia et Cosmochimica Acta 64 (9), 1557–1565. https://doi.org/10.1016/S0016-7037(99)00400-7.
Wei, W., Algeo, T.J., 2020. Elemental proxies for paleosalinity analysis of ancient shales and mudrocks.pdf. Geochimica et Cosmochimica Acta 287, 341–366. https://doi.org/10.1016/j.gca.2019.06.034.
Wilkin, R.T., Barnes, H.L., 1996. Pyrite formation by reactions of iron monosulfides with dissolved inorganic and organic sulfur species. Geochimica et Cosmochimica Acta 60, 4167–4179. https://doi.org/10.1016/s0016-7037(97)81466-4.
Wilkin, R.T., Barnes, H.L., 1997. Formation processes of framboidal pyrite. Geochimica et Cosmochimica Acta 61, 323–339. https://doi.org/10.1016/s0016-7037(96)00320-1.
Wilkin, R.T., Barnes, H.L., Brantley, S.L., 1996. The size distribution of framboidal pyrite in modern sediments: an indicator of redox conditions. Geochimica et Cosmochimica Acta 60 (20), 3897–3912. https://doi.org/10.1016/0016-7037(96)00209-8.
Wintsch, R.P., Kvale, C.M., 1994. Differential mobility of elements in burial diagenesis of siliciclastic rocks. Journal of Sedimentary Research 64, 349–361. https://doi.org/10.1306/d4267d9d-2b26-11d7-8648000102c1865d.
Wissler, L., Funk, H., Weissert, H., 2003. Response of Early Cretaceous carbonate platforms to changes in atmospheric carbon dioxide levels. Palaeogeography Palaeoclimatology Palaeoecology 200, 187–205. https://doi.org/10.1016/s0031-0182(03)00450-4.
Wolgemuth, K., Broecker, W.S., 1970. Barium in sea water. Earth and Planetary Science Letters 8, 372–378. https://doi.org/10.1016/0012-821x(70)90110-x.
Wright, J., Schrader, H., Holser, W.T., 1987. Paleoredox variations in ancient oceans recorded by rare earth elements in fossil apatite. Geochimia et Cosmochimia Acta 51, 631–644. https://doi.org/10.1016/0016-7037(87)90075-5.
Young, R.A., 1993. Introduction to the Rietveld method. The Rietveld Method. Oxford University Press, Oxford.
Zeiler, R., 1902. Sobre las impresiones vegetales del Kimeridgense de santa Maria de Meya. Memorias de la Real Academia de Ciencias y Artes de Barcelona 4 (26), 345–356.